Supplementary Information

Continuous direct air capture and conversion tandem system applicable to a wide range of CO_2 concentrations

Shinta Miyazaki[a], Akihiko Anzai[a,*], Masaki Yoshihara[a], Hsu Sheng Feng[a], Shinya Mine[b], Takashi Toyao[a], Ken-ichi Shimizu[a,*]

[a] Institute for Catalysis, Hokkaido University, N-21, W-10, Sapporo 001-0021, Japan

[b] Research Institute for Chemical Process Technology, National Institute of Advanced Industrial Science and Technology (AIST), 4-2-1, Nigatake, Miyagino-ku, Sendai 983-8551, Japan

*Corresponding author
Akihiko Anzai, E-mail: anzai.akihiko@cat.hokudai.ac.jp
Ken-ichi Shimizu, Email: kshimizu@cat.hokudai.ac.jp

Supplementary Figures and Texts

1 Introduction

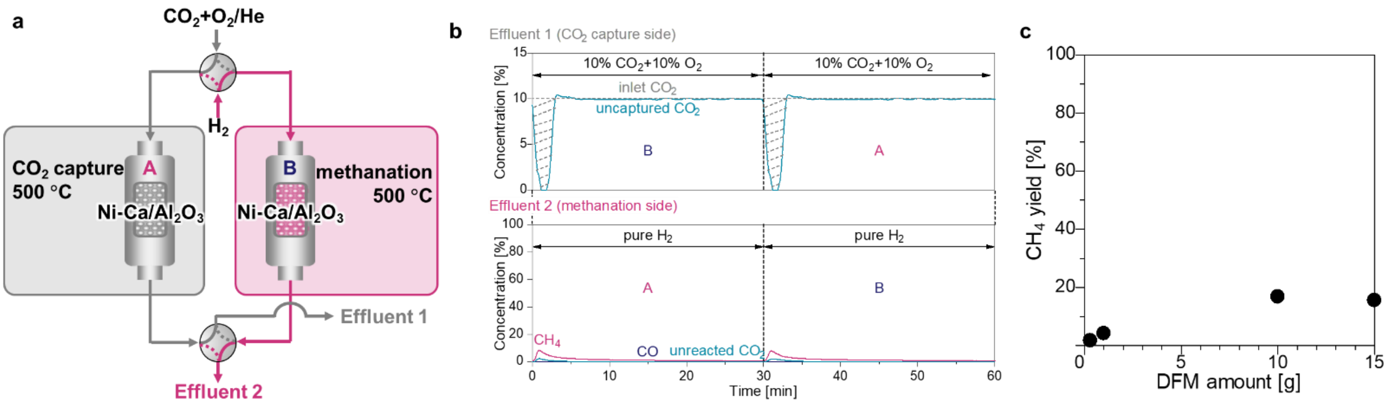

Fig. S1 a. Schematic diagram of the continuous CO_2 capture and methanation system; captured gas (100 mL/min, 10%CO_2+10%O_2/He for 30 min) and hydrogenation gas (100 mL/min, pure H_2 for 30 min) were alternately fed into each reactor containing 10 g of Ni-Ca/Al_2O_3 **b**. Typical time course of the CH_4, CO_2, and CO concentration in effluent 1 and 2, respectively. **c**. Variation in CH_4 yield with DFM amount in continuous CO_2 capture and methanation.

Text S1

Previously, various DFMs for selective CH_4 production were reported. Especially, Ni-Ca based DFMs were well-known as high performance one (Table S1 and S2). Recently, our group developed Ni-Ca/Al_2O_3 DFM, which optimized Ni and Ca loading. Detail characterization revealed that 500 ºC is the best condition for CO_2 capture and methanation. For continuous CH_4 production from high concentration of CO_2, we carried out CO_2 capture and methanation using the continuous CCR system (Fig. S1a). First, the CO_2/O_2 mixture was fed into one reactor for 30 min for CO_2 capture. On the other hand, pure H_2 was fed into the other reactor (containing a CO_2-captured Ni-Ca/Al_2O_3). Fig. S1b shows the typical time course of the CH_4, and CO_2 concentrations analyzed by online gas-cell IR in effluent 1 and 2, respectively. Fig. S1c shows the result of the optimization of Ni-Ca/Al_2O_3 amount. These results indicate that increasing the amount of DFM has limited effects on improving CH_4 yield (<20%).

Text S2

The conventional stepwise CCR system illustrated in Fig. 1a was originally developed by Farrauto's group, who pioneered the concept[†]. They successfully demonstrated the capture of CO_2 from emission sources and its subsequent conversion to CH_4 within a single reactor at the same temperature (320 °C), using Ru and nano-dispersed CaO co-supported on porous γ-Al_2O_3. Around the same period, Urakawa's group demonstrated CO_2 capture and subsequent hydrogenation to CO using a DFM composed of earth-abundant elements (FeCrCu/K/MgO–Al_2O_3) [‡]. Furthermore, they proposed a continuous operation concept, illustrated in Fig. 1b, in which CO_2 can be continuously removed from the effluent stream and converted into valuable products (such as syngas) by synchronizing the switching of gas flow directions between two reactors with an appropriate time delay. Following these pioneering studies, our group demonstrated continuous CCR to CO using a dual-functional material composed of Pt nanoparticles coordinated with Na oxides on Al_2O_3, integrated within a reactor configuration similar to that shown in Fig. 1b[¶]. Our previous study demonstrated a groundbreaking CCR process that promotes CO_2 capture and reduction at significantly lower temperatures compared to conventional systems. However, it had a limitation in effectively capturing high concentrations of CO_2, such as those found in simulated exhaust gas. To address this issue, we developed a new process configuration, as shown in Fig. 1c, by integrating a TSA system capable of capturing large amounts of CO_2.

† M. Duyar, M. Treviño, R. Farrauto, *Appl. Catal. B:*, 2015, 168-169, 370-376

‡ L. Bobadilla, J. Riesco-García, G. Penelás-Pérez, A. Urakawa, *J. CO2 Util.*, 2016, 14, 106-111

¶ S. Miyazaki, L. Li, S. Yasumura, K. Ting, T. Toyao, Z. Maeno, K. Shimizu, *ACS Catal.*, 2022, 12, 2639−2650

2 Results and Discussion

2.1 Screening and optimization of sorbents and catalysts

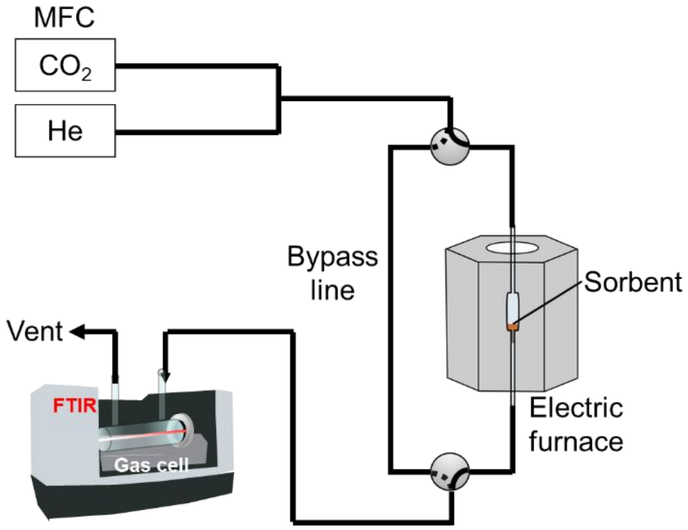

Fig. S2 Illustration of the experimental setup for CO_2 adsorption measurement.

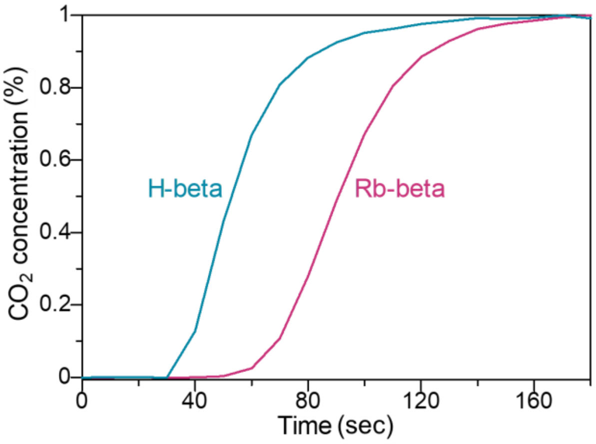

Fig. S3 Profile of the breakthrough experiments over H-beta and Rb-beta under a flow of 1% CO_2 at 50 °C, total flow rate = 100 mL/min, He balance. Weight of adsorbents: 100 mg. The feed gases were introduced to the adsorbents from 0 s.

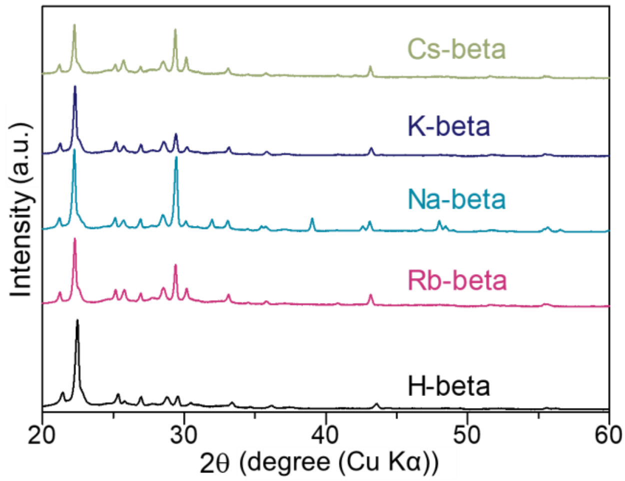

Fig. S4 XRD patterns of H-beta, Rb-beta, Na-beta, K-beta, and Cs-beta.

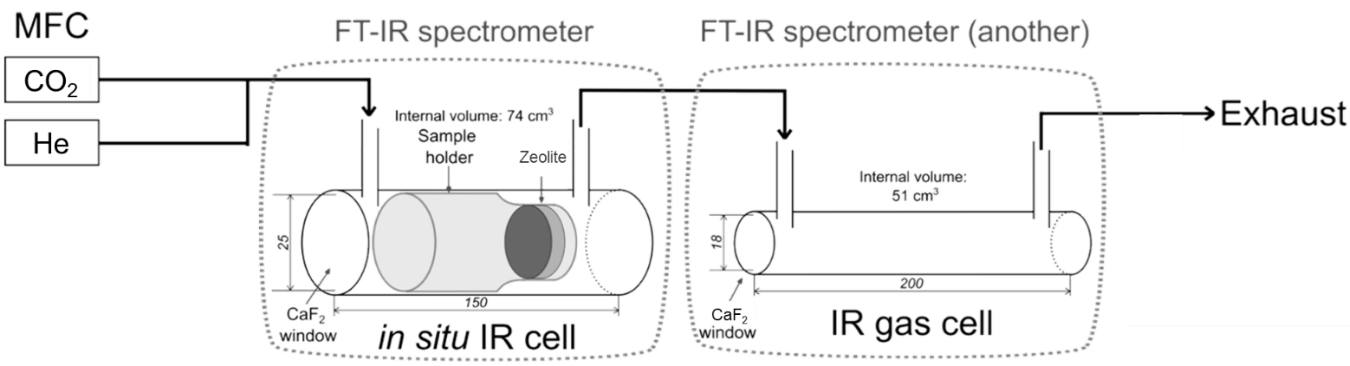

Fig. S5 Schematic view of the setup used for *operando* IR measurement, including *in situ* IR cell and IR gas cell. The inner diameter and length of the cell are provided with a unit of mm.

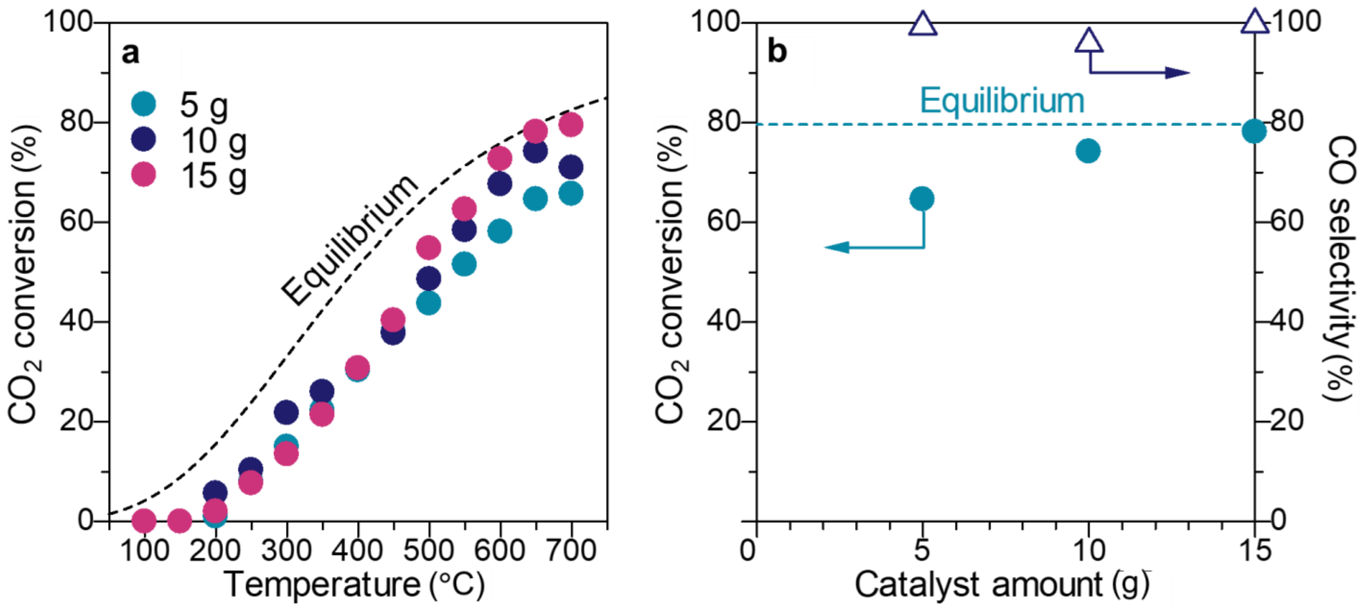

Fig. S6 a. Validation in CO_2 conversion with respect to temperature for different amounts of $Cu/ZnO/Al_2O_3$. **b,** Variation in CO_2 conversion and CO selectivity with catalyst amount in steady-state RWGS reaction over $Cu/ZnO/Al_2O_3$.

2.2 Continuous production of O_2-free CO_2 from CO_2/O_2 mixture

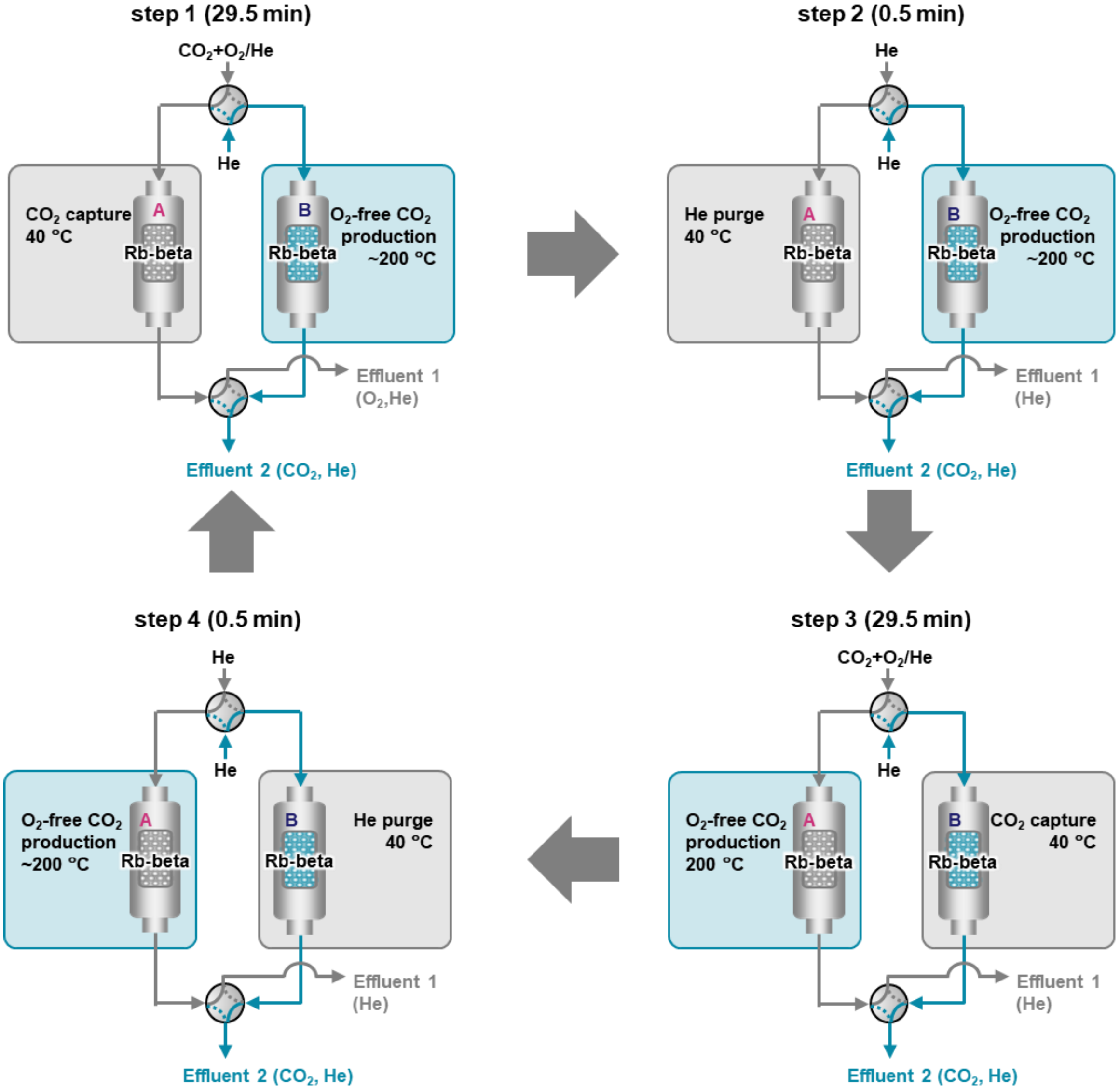

Fig. S7 Schematic diagram and procedure of the continuous CO_2 capture and O_2-free CO_2 production.

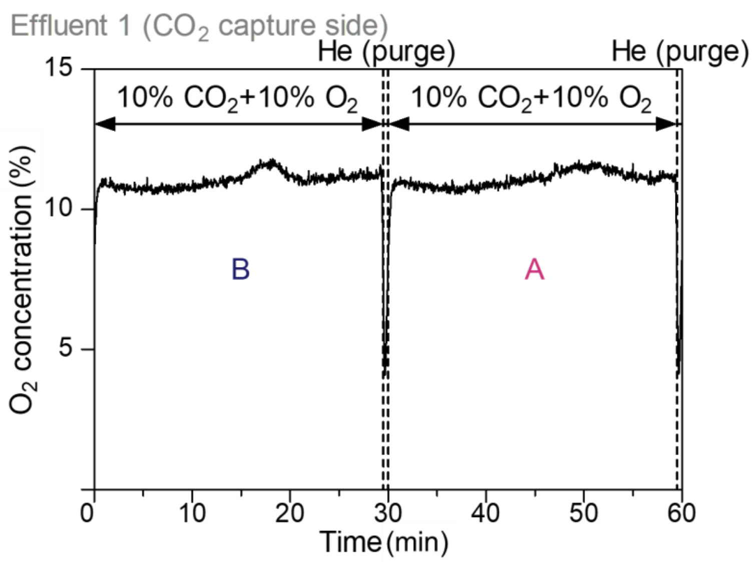

Fig. S8 Typical time course of the O_2 concentration in effluent 1 during continuous CO_2 capture and O_2-free CO_2 production.

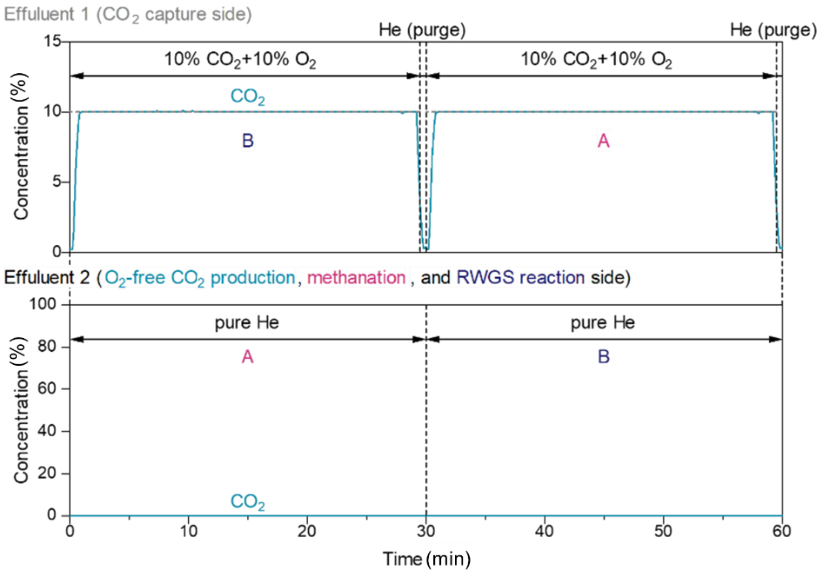

Fig. S9 Effluent concentration profiles of CO_2 for blank during continuous CO_2 capture and O_2-free CO_2 production, methanation and. RWGS reaction side production; captured gas (100 mL min^{-1}, 10%CO_2+10%O_2/He for 29.5 min and then pure He for 0.5 min) and other side gas (120 mL min^{-1}, pure He for 30 min).

Text S3

In continuous CO_2 capture and O_2-free CO_2 production, the total flow rate was moderately changed due to O_2-free CO_2 production. The total flow rate in effluent 2 can be shown eq. 1. The produced O_2-free CO_2 flow rate can be calculated in eq. 2. Finally, eq. 3 to derive the total flow rate was calculated from eqs. 1 and 2. The derived total flow rate is close to the measured total flow rate by the soap-film flow meter (HORIBA, Ltd., Fluid Control System SF-1U combined VP-3U, Fig. S7). From eqs. 2 and 6, the amount of produced O_2-free CO_2 every 0.5 min was derived and O_2-free CO_2 yield was also calculated (O_2-free CO_2 yield = 97%, Fig. S7).

$$F_{all}^{out(2)} = F_{CO2}^{out(2)} + F_{He}^{out(2)} \quad (1)$$

$$F_{CO2}^{out(2)} = C_{CO2}^{out(2)} \times F_{all}^{out(2)} \quad (2)$$

$$F_{all}^{out(2)} = \frac{F_{He}^{out(2)}}{1-C_{CO2}^{out(2)}} \quad (3)$$

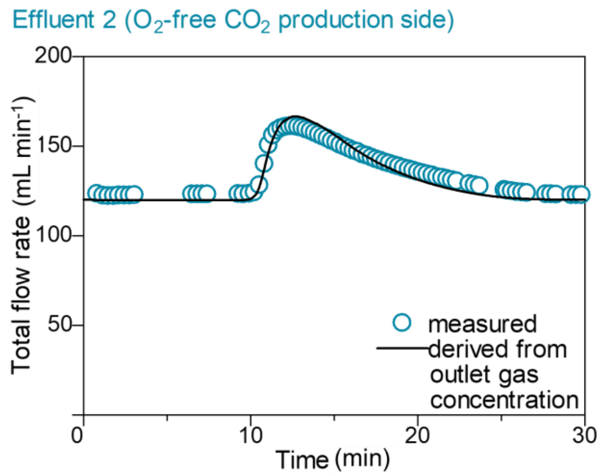

Fig. S10 Comparison of changes about measured total flow rate and derived total flow rate from outlet gas concentration in effluent 2 during CO_2 capture and O_2-free CO_2 production. Conditions are the same as in Fig. 5. The methodology of total flow rate derivation from outlet gas concentration in effluent 2 is shown in Supplementary Text 1.

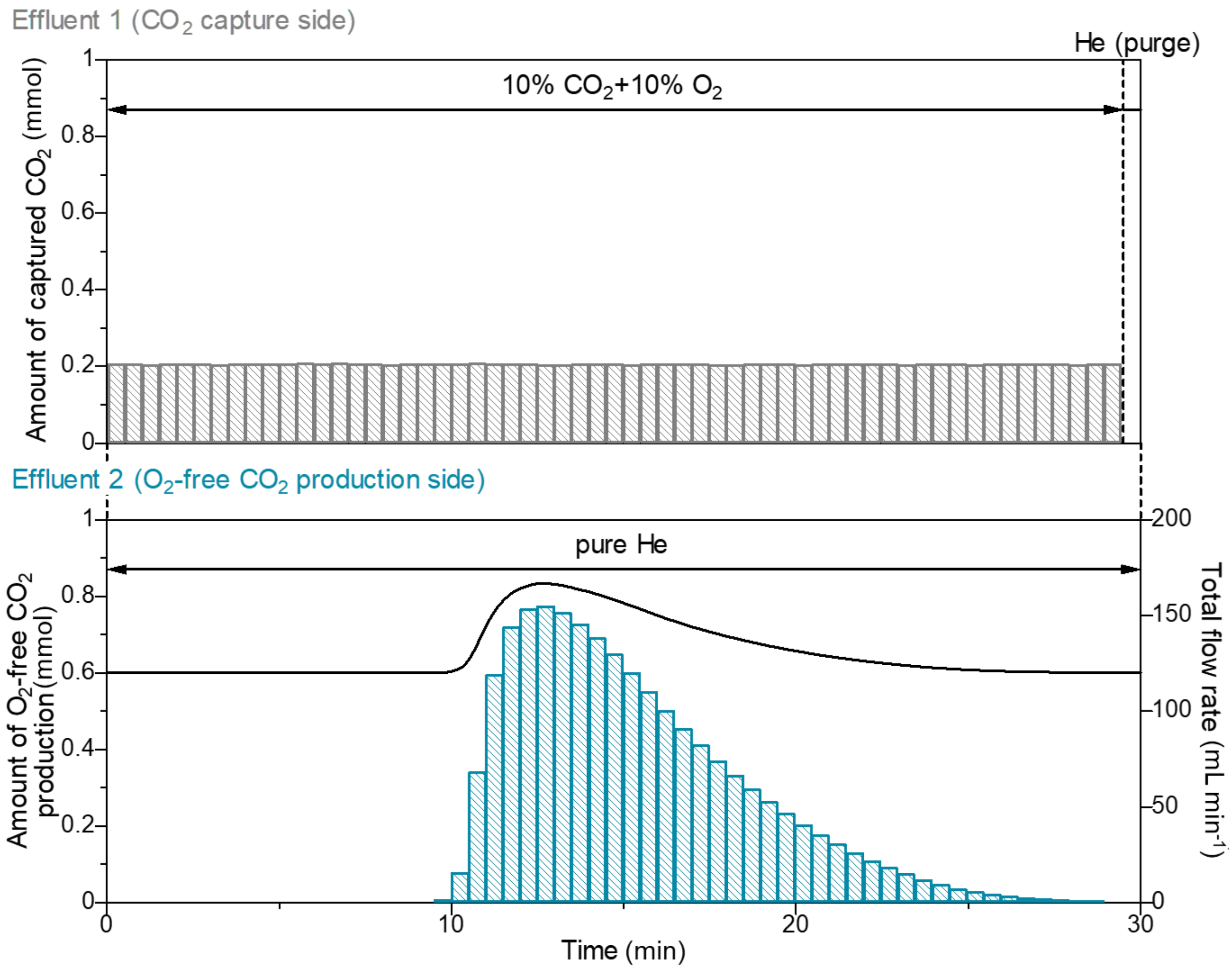

Fig. S11 Time course of amount of captured CO_2 in effluent 1, O_2-free CO_2 production in effluent 2 every 0.5 min, and total flow rate of effluent 2 for continuous CO_2 capture and RWGS reaction. Conditions are the same as in Fig. 5.

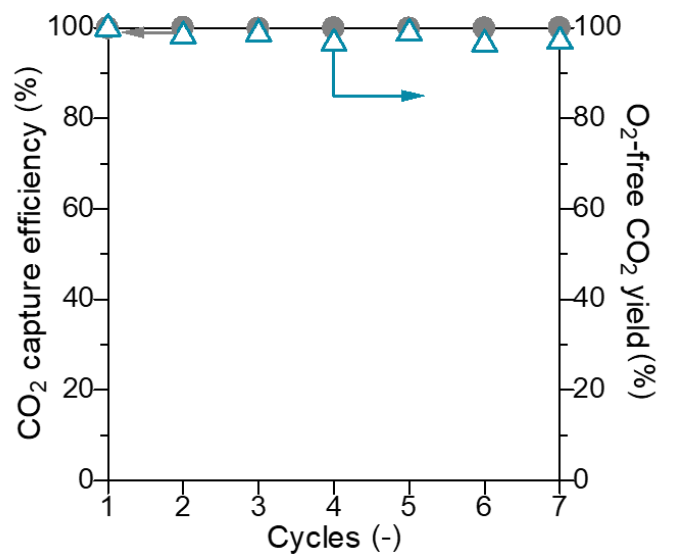

Fig. S12 Transitions of the CO_2 capture efficiency and O_2-free CO_2 yield during cyclic test of continuous CO_2 capture and O_2-free CO_2 production. Conditions are the same as in Fig. 5.

2.3 Continuous CO_2 capture and methanation/RWGS reaction using the tandem system

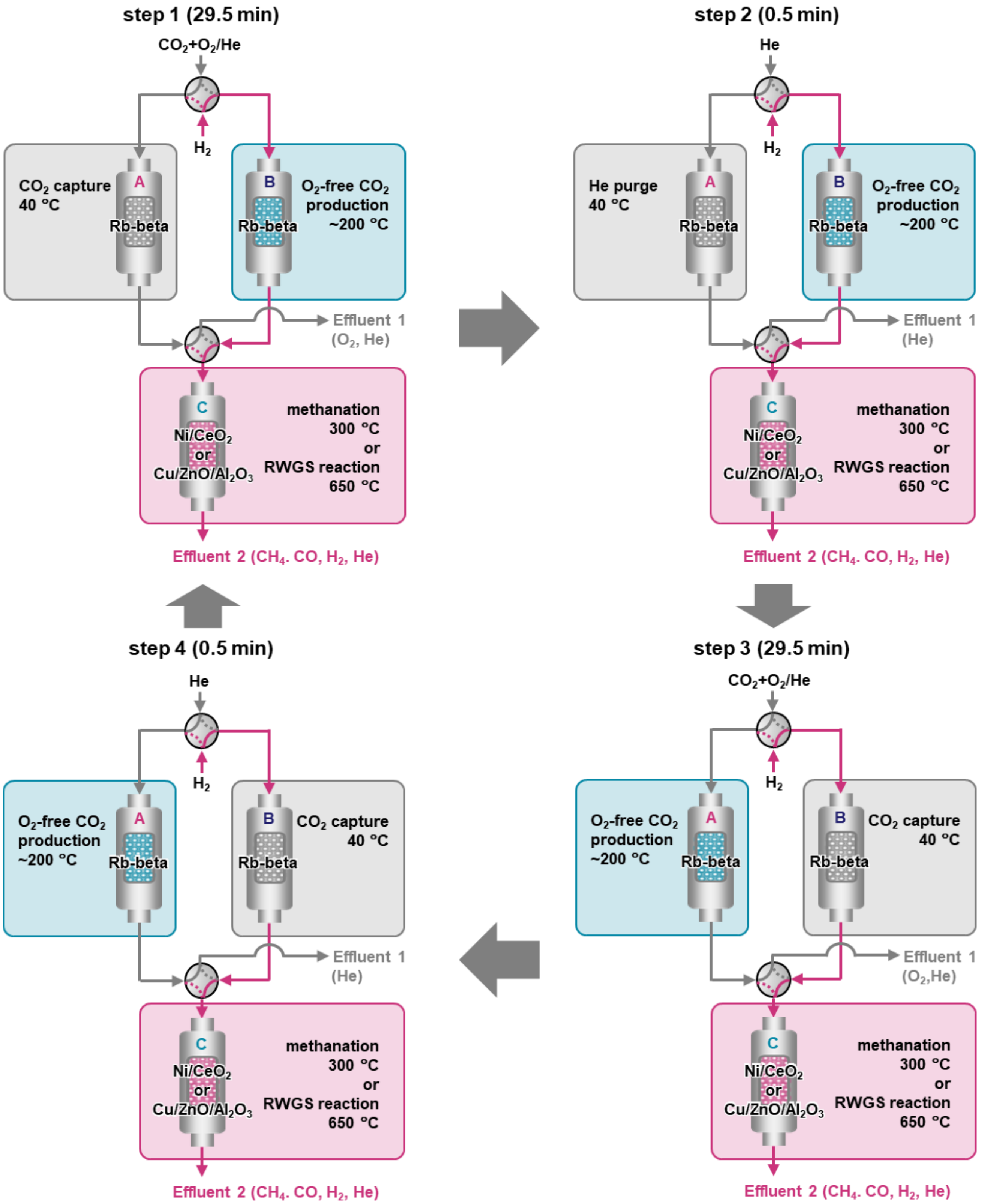

Fig. S13 Schematic diagram and procedure of the continuous CO_2 capture and methanation as well as RWGS reaction.

Text S4

In continuous high-concentration CO_2 capture and methanation, total flow rate was drastically changed due to large amount of CH_4 formation. The total flow rate in effluent 2 can be shown eq. 1, because of produced CO and unreacted CO_2 are hardly observed, and produced H_2O was captured by the cold trap. From the stochiometric equation of methanation (eq. 3 in Main Text), produced CH_4 and unreacted H_2 flow rates can be shown eqs. 2 and 3, respectively. amount of converted H_2 can be calculated by eq. 4 and eq. 4 can transformed to eq. 5 using eq. 2. Finally, eq. 6 to derive the total flow rate was calculated from eqs. 4 and 5. The derived total flow rate is close to the measured total flow rate by the soap-film flow meter (HORIBA, Ltd., Fluid Control System SF-1U combined VP-3U). From eqs. 2 and 6, the amount of produced CH_4 every 0.5 min was derived and CH_4 yield was also calculated (CH_4 yield = 92%, Fig. S10).

$$F_{all}^{out(2)} = F_{CH4}^{out} + F_{H2}^{out} \quad (1)$$

$$F_{CH4}^{out} = C_{CH4}^{out} \times F_{all}^{out(2)} \quad (2)$$

$$F_{H2}^{out} = (1 - C_{CH4}^{out}) \times F_{all}^{out(2)} \quad (3)$$

$$F_{H2}^{in} - F_{H2}^{out} = 4 \times F_{CH4}^{out} \quad (4)$$

$$F_{H2}^{in} - F_{H2}^{out} = 4 \times C_{CH4}^{out} \times F_{all}^{out(2)} \quad (5)$$

$$F_{all}^{out} = \frac{F_{H2}^{in}}{1+3C_{CH4}^{out}} \quad (6)$$

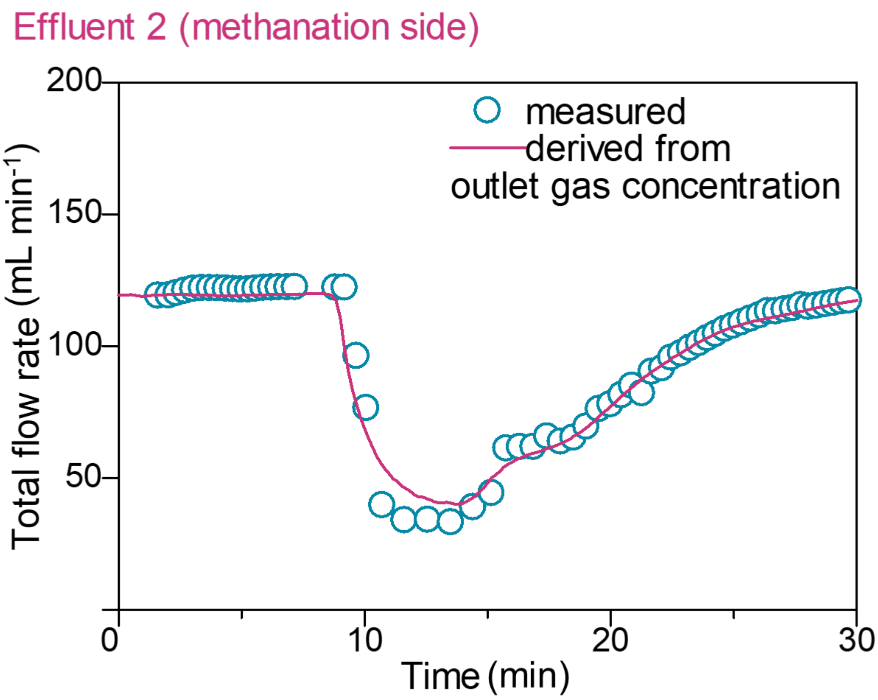

Fig. S14 Comparison of changes about measured total flow rate and derived total flow rate from outlet gas concentration in effluent 2 during CO_2 capture and methanation. Conditions are the same as in Fig. 5. The methodology of total flow rate derivation from outlet gas concentration in effluent 2 is shown in Supplementary Text 3.

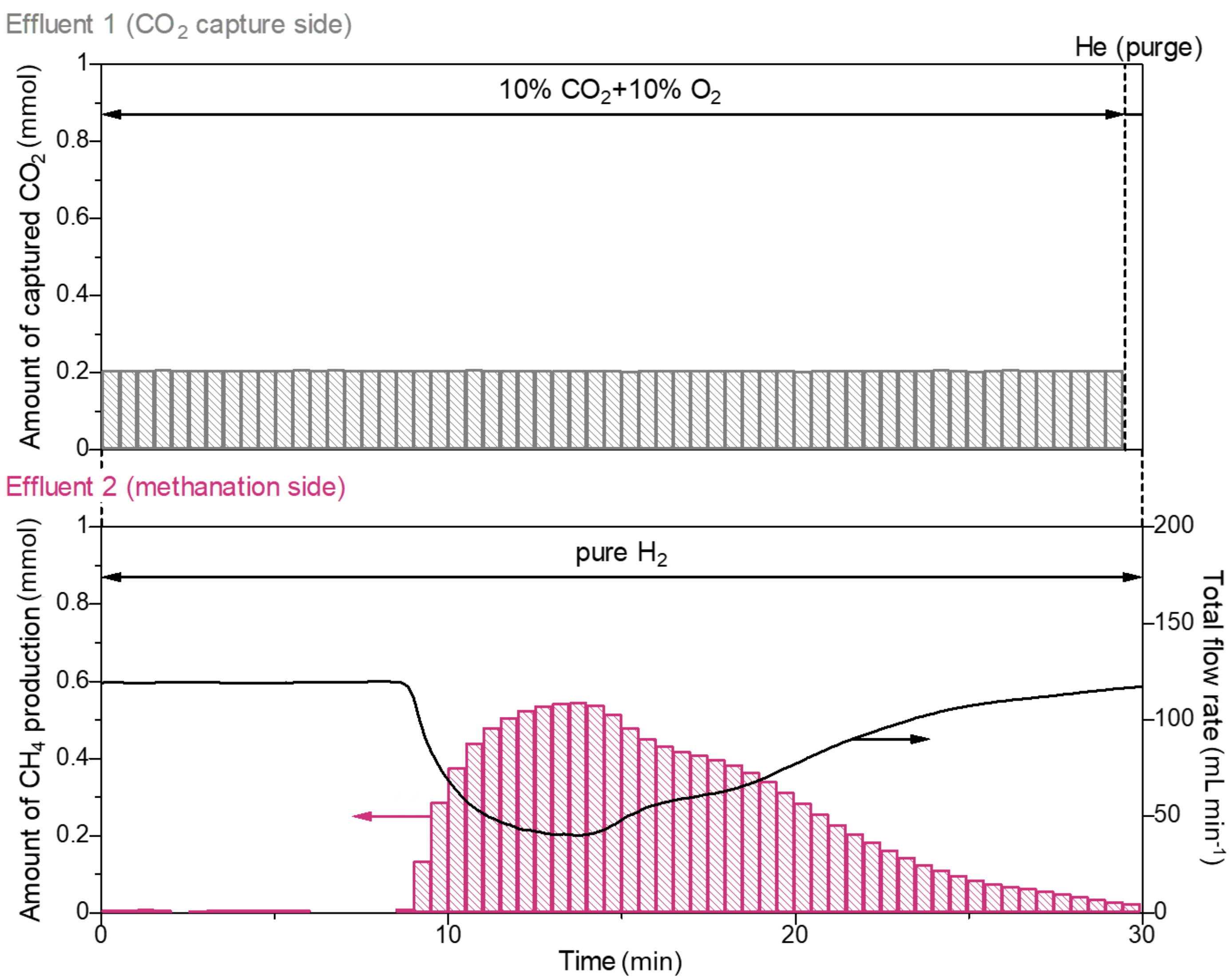

Fig. S15 Time course of amount of captured CO_2 in effluent 1, CH_4 production in effluent 2 every 0.5 min, and total flow rate of effluent 2 for continuous CO_2 capture and methanation. Conditions are the same as in Fig. 5.

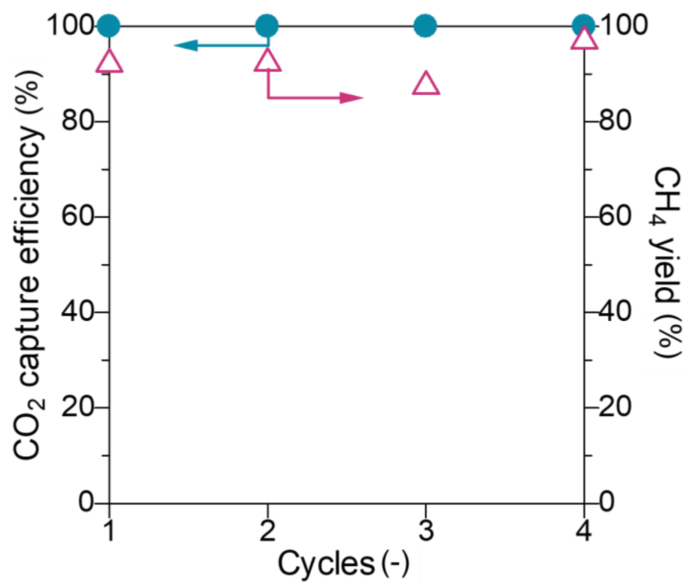

Fig. S16 Transitions of the CO_2 capture efficiency and CH_4 yield during cyclic test of continuous CO_2 capture and RWGS reaction. Conditions are the same as in Fig. 5.

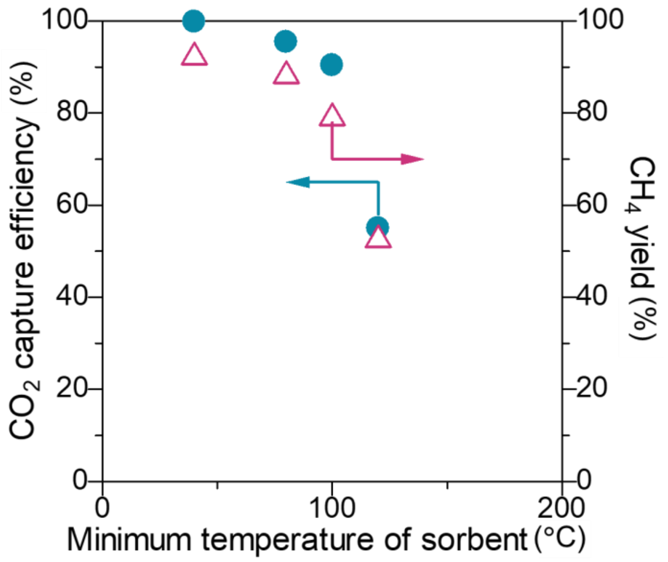

Fig. S17 Variation in CO_2 capture efficiency and CH_4 yield with range of temperature changing (minimum range from 40 °C to 120 °C) in continuous CO_2 capture and CH_4 production.

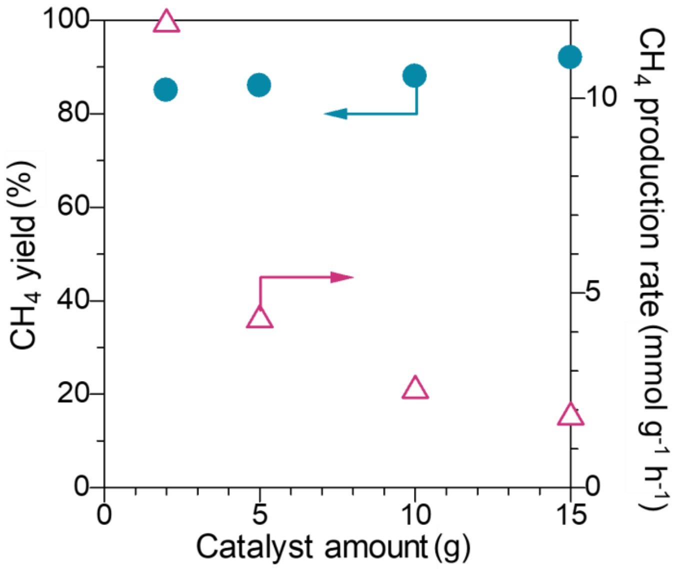

Fig. S18 Variation in CH_4 yield and CH_4 production rate with catalyst amount in continuous CO_2 capture and CH_4 production.

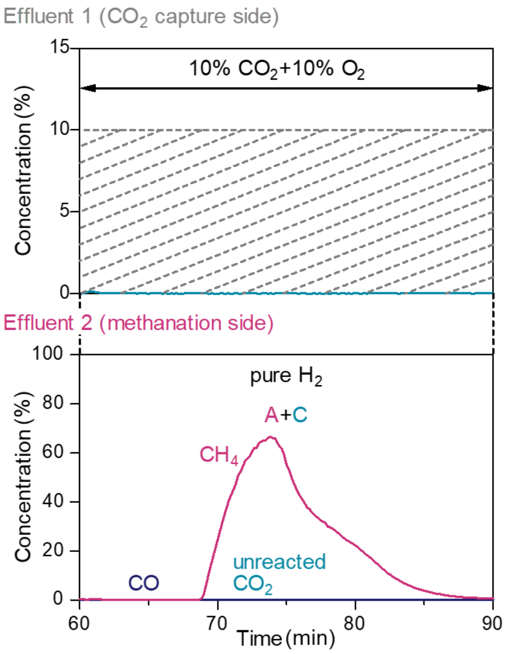

Fig. S19 Typical time course of uncaptured CO_2 in effluent 1 and CH_4, CO, and unreacted CO_2 in effluent 2 for continuous CO_2 capture and methanation under process-relevant conditions (without He purge). Conditions: 14 g of Rb-beta for each upper reactor, temperature swing from 40 °C to 200 °C (heating rate = 5.5 °C/min). 15 g of Ni/CeO_2 for the bottom reactor, 300 °C. 100 mL/min 10% CO_2+10% O_2/He for 30 min, switched to 120 mL/min H_2 for another 30 min.

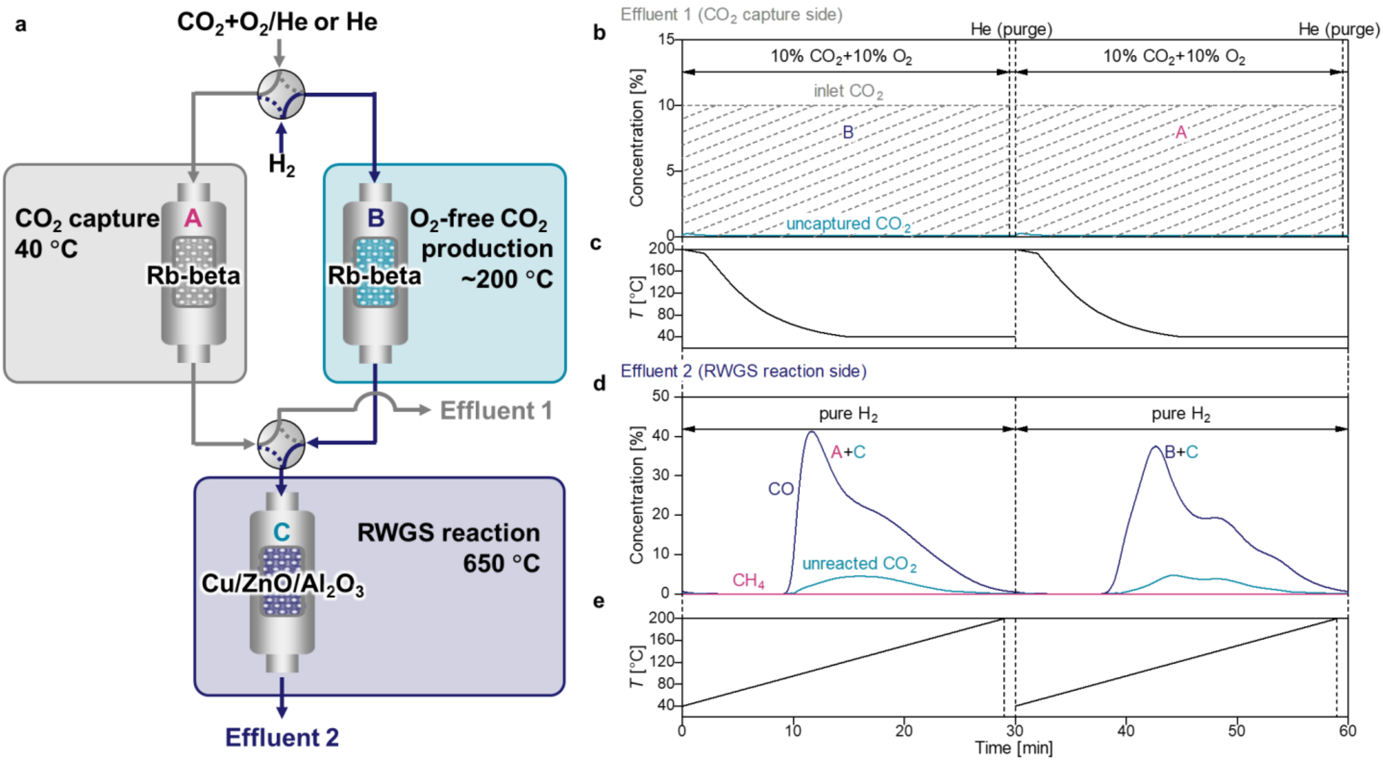

Fig. S20 (a) Schematic diagram of the two-reactor TSA system for continuous CO_2 capture and RWGS reaction; captured gas (100 mL/min, 10%CO_2+10%O_2/He for 29.5 min and then pure He for 0.5 min) and hydrogenation gas (100 mL/min, pure H_2 for 30 min) were alternately fed into each reactor containing 14 g of Rb-beta (b and d) Typical time course of the CO_2 and O_2 concentration in effluent 1 and 2, respectively. (c and e) Typical time course of the temperature changing in reactor a and b, respectively.

Text S5

In continuous high-concentration CO_2 capture and RWGS reaction, total flow rate was slightly changed due to CO formation and CO_2 desorption. Using the soap-film flow meter, total flow rate in effluent 2 was measured and the amount of produced CO every 0.5 min was derived, and CO yield was also calculated (CO yield = 85%, Fig. S18).

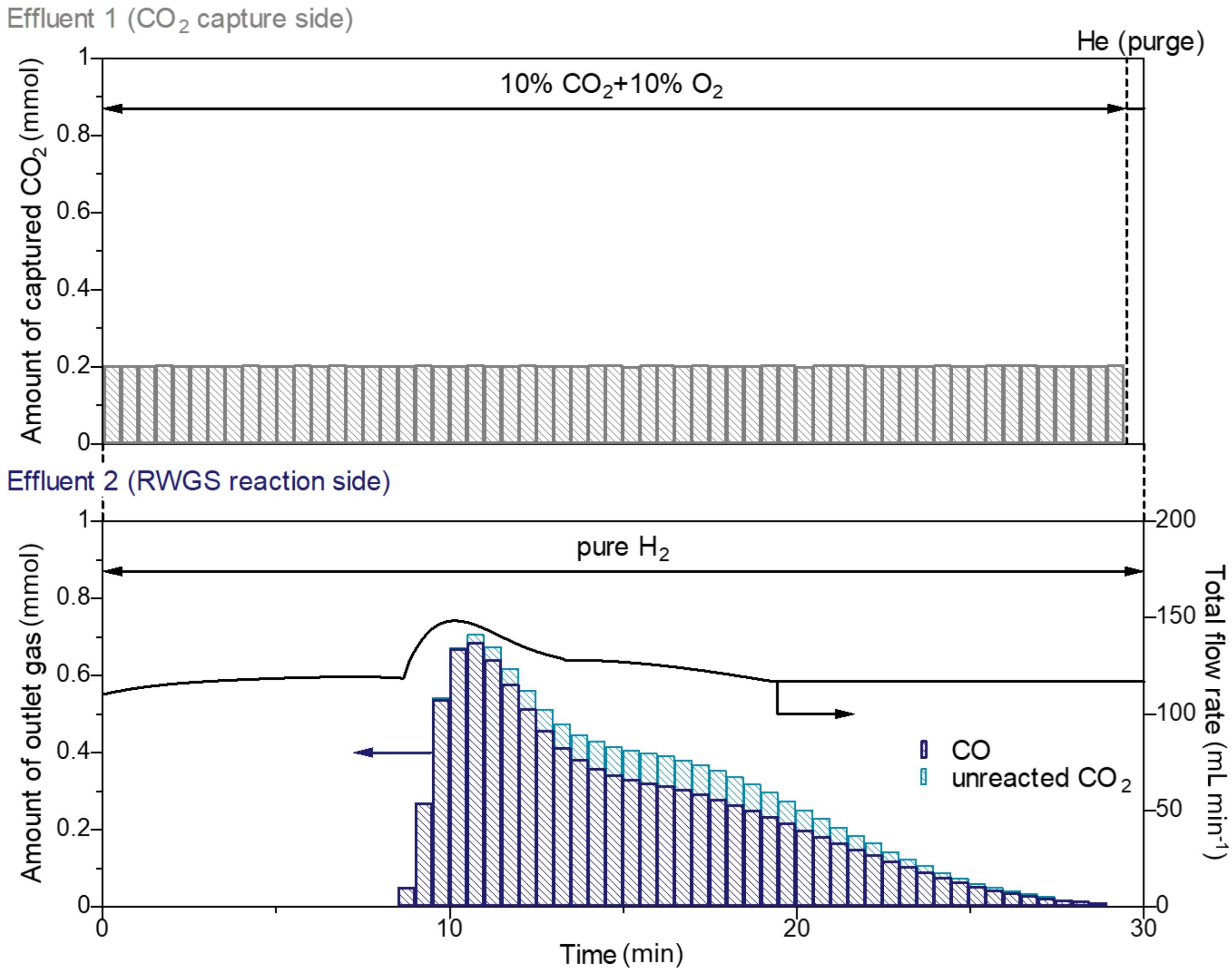

Fig. S21 Time course of amount of captured CO_2 in effluent 1, CO production in effluent 2 every 0.5 min, and total flow rate of effluent 2 for continuous CO_2 capture and RWGS reaction. Conditions are the same as in Fig. S17.

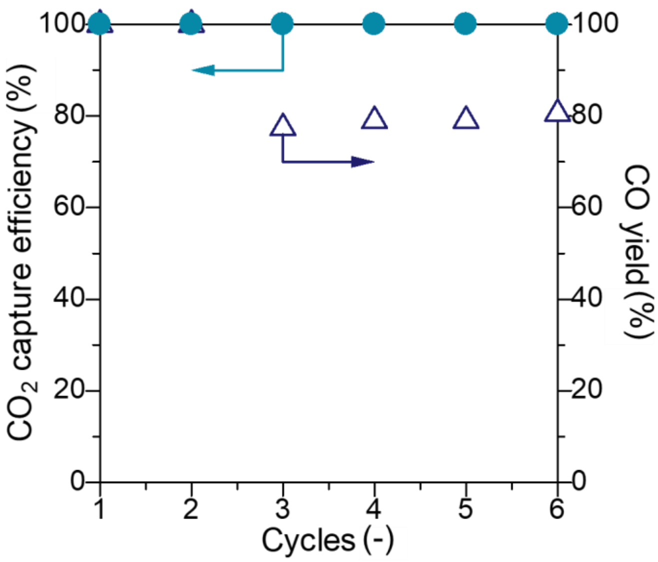

Fig. S22 Transitions of the CO_2 capture efficiency and CO yield during the cyclic test of continuous CO_2 capture and RWGS reaction. Conditions are the same as in Fig. S17.

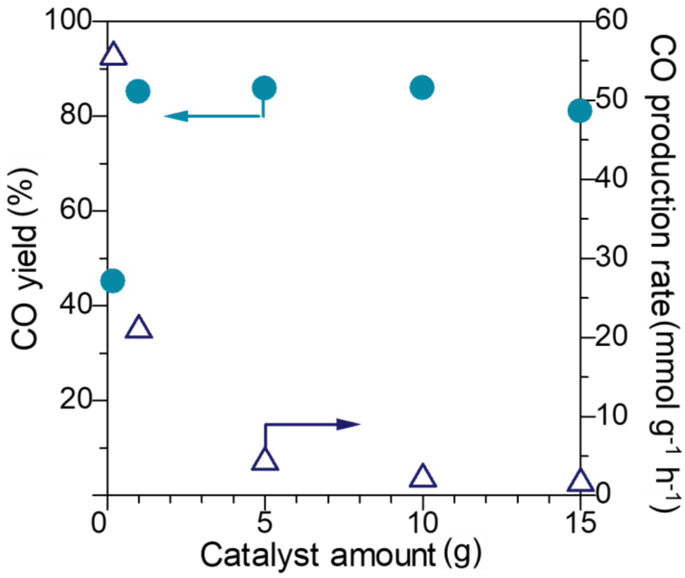

Fig. S23 Variation in CO yield and STY_{CO} with catalyst amount in continuous CO_2 capture and RWGS Reaction.

Text S6

H_2 conversion is also an important property in the CO_2 methanation process. We demonstrated continuous CO_2 capture and methanation, with the H_2 flow time of H_2 reduced from 30 min to 20 min. Similar to Fig. 6, 10% CO_2 + 10% O_2 was fed into one reactor for 29.5 min for CO_2 capture with cooling, and then pure He (0.5 min) was fed to purge the remaining O_2 in the reactor and gas line (Fig. S24a). At the same time, into the other reactor in parallel, pure H_2 was fed at 20 min after 10 min of no gas flow with heating. CO_2 capture efficiency and CH_4 yield were maintained during 4 cycles at 99% and 93%, respectively (Fig. S24e). The effect of H_2 flow time was investigated and H_2 conversion and the average CH_4 concentration were increased from 38% to 58%, and from 9.8% to 15%, respectively.

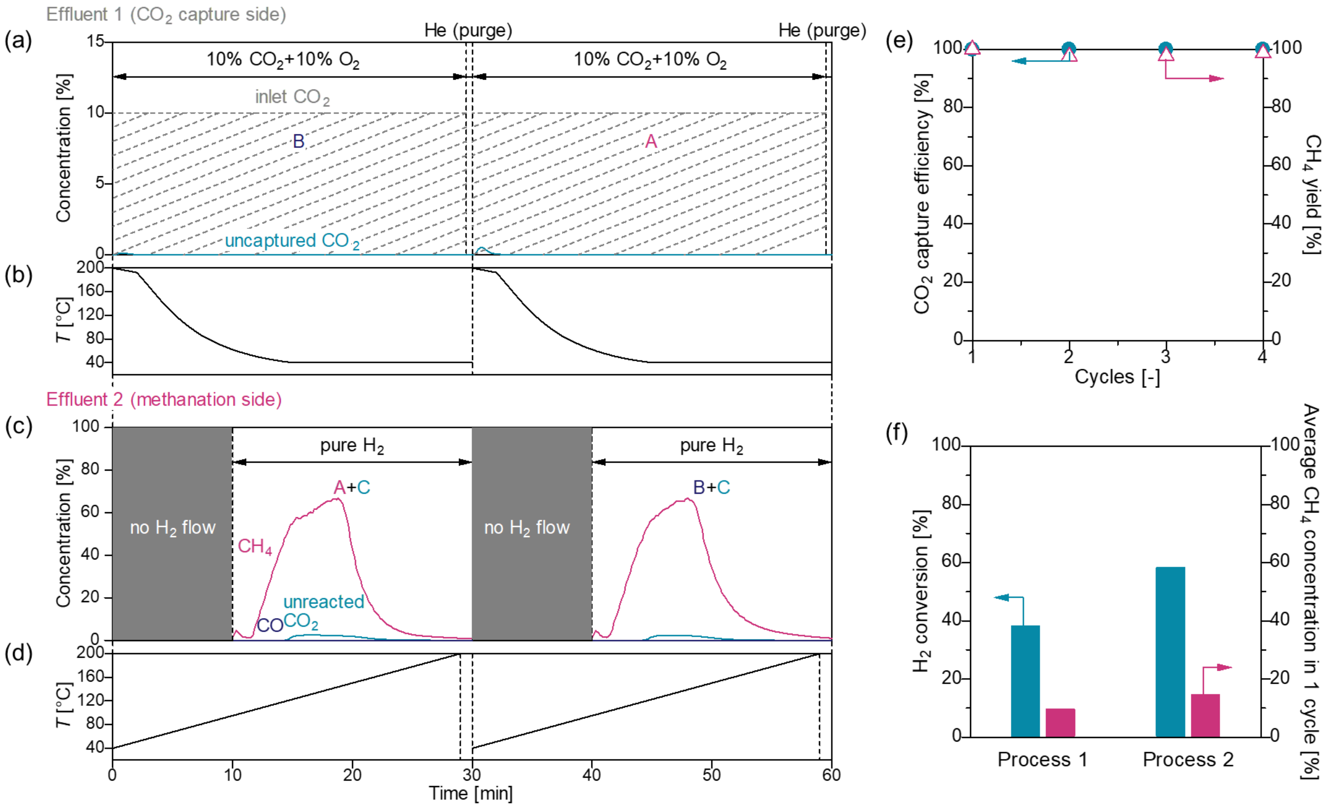

Fig. S24 Continuous CO_2 capture and methanation; captured gas (100 mL min^{-1}, 10% CO_2+10%O_2/He for 29.5 min and then pure He for 0.5 min) and hydrogenation gas (100 mL min^{-1}, pure H_2 for 20 min) were alternately fed into each reactor containing 14 g of Rb-beta. (a and c) Typical time course of the CH_4, CO_2, and CO concentration in effluent 1 and 2, respectively. (b and d) Typical time course of the temperature changing in reactor a and b, respectively. (e) Transitions of the CO_2 capture efficiency and CH_4 yield during cyclic test. (f) Comparison of H_2 conversion and average CH_4 concentration in 1 cycle between conditions of Fig. 6 (denoted as process 1) and conditions of Fig. S24 (denoted as process 2).

2.4 Continuous direct air capture and methanation

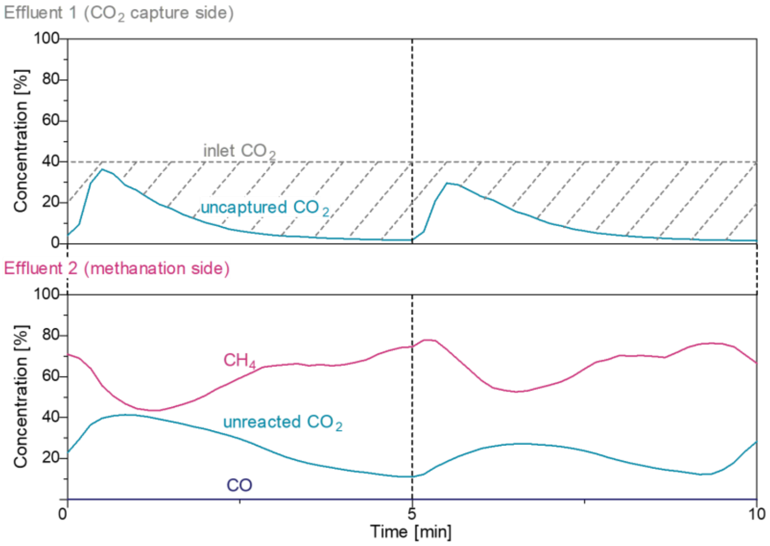

Fig. S25 Typical time course of uncaptured CO_2 in effluent 1 and CH_4, CO, and unreacted CO_2 in effluent 2 for continuous high-concentration CO_2 capture and methanation. Conditions: 14 g of Rb-beta for each upper reactor, temperature swing from 80 °C to 100 °C (heating rate = 20 °C/min). 15 g of Ni/CeO_2 for the bottom reactor, 300 °C. 500 mL/min air for 5 min, switched to 10 mL min^{-1} H_2 for another 5 min.

2.5 Energy efficiency

Text S7

The energy efficiency (denoted as η) was defined as the ratio between the outlet energy based on the low heating value (LHV) of CH_4 and the overall energy. For example, Andrew et al. evaluated the η of CO_2 methanation under both pseudo-adiabatic and adiabatic configurations, and demonstrated that the adiabatic configuration significantly enhances the overall efficiency of the methanation process[†]. While the definition of η excludes the contribution of the LHV of unreacted H_2, it serves as a reliable metric for evaluating and comparing the efficiency of CO_2 conversion. In contrast, the fuel production efficiency (FPE) is defined as the ratio of the total output energy to the total input energy. Both input and output energies were calculated based on the LHV and the applied electrical power (P). Murphy et al. demonstrated a linear correlation between the flow rate–normalized input energy and the fuel production efficiency (FPE)[‡], highlighting the utility of FPE as an indicator of how effectively CO_2 and H_2 are jointly converted into higher-value energy outputs.

† M. Biset-Peiróa, R. Meyb, J. Guileraa, and T. Andreua, *Chem. Eng. J.* 2020, **393**, 124786

‡ S. Ullah, Y. Gao, L. Dou, Y. Liu, T. Shao, Y. Yang and A. B. Murphy, *Plasma Chemistry and Plasma Processing*, 2023, **43**, 1335–1383.

Tables

2 Results and Discussion

Table S1. Summary of the continuous CO_2 capture and methanation in this study and other reported CO_2 capture and methanation considering the effect of coexistent O_2. Entries without *, †, or ‡ symbols using Fig. 1a system.

DFMs or catalyst	CO_2 capture gas	Hydrogenation gas	CH_4 yield [%]	*T* [°C]	ref
Ni(5)/CeO_2*	10%CO_2+10%O_2/He	100% H_2	92	300	*
Ru(1)-Ni(10)-Na_2O(6.1) /Al_2O_3	7.5%CO_2+4.5%O_2 +15%H_2O/N_2	15%H_2/N_2	5.67	320	[1]
Pt(1)-Ni(10)-Na_2O(6.1) /Al_2O_3	7.5%CO_2+4.5%O_2 +15%H_2O/N_2	15%H_2/N_2	3.73	320	[1]
Ru(1)-Na_2O(6.1) /Al_2O_3	7.5%CO_2+4.5%O_2 +15%H_2O/N_2	15%H_2/N_2	4.63	320	[1]
Ru(5)-Na_2O(6.1) /Al_2O_3	7.5%CO_2+4.5%O_2 +15%H_2O/N_2	15%H_2/N_2	4.35	320	[2]
Ni(10)-Na_2O(6.1) /Al_2O_3	7.5%CO_2+4.5%O_2 +15%H_2O/N_2	15%H_2/N_2	4.12	320	[2]
Ru(0.95)-K(5) /Al_2O_3	1%CO_2+3%O_2+ 2.5%H_2O/He	4%H_2/He	0.38	350	[3]
Ru(0.95)-Ca(5.1) /Al_2O_3	1%CO_2+3%O_2 +2.5%H_2O/He	4%H_2/He	0.48	350	[3]
Ru(0.84)-Ba(16) /Al_2O_3	1%CO_2+3%O_2 +2.5%H_2O/He	4%H_2/He	2.22	350	[3]
Ni(10)-Ca(30)/Al_2O_3†	1%CO_2+10%O_2/N_2	100%H_2	0.15	450	[4]
Ni(10)/Al_2O_3†	1%CO_2+10%O_2/N_2	100%H_2	0.002	450	[4]
Ni(10)-Ca(6)/Al_2O_3†	1%CO_2+10%O_2/N_2	100%H_2	0.08	450	[4]
Ni(10)-Ca(20)/Al_2O_3†	1%CO_2+10%O_2/N_2	100%H_2	0.09	450	[4]
Ni(10)-Ca(40)/Al_2O_3†	1%CO_2+10%O_2/N_2	100%H_2	0.15	450	[4]
Ni(5)-Ca(30)/Al_2O_3†	1%CO_2+10%O_2/N_2	100%H_2	0.13	450	[4]
Ni(20)-Ca(30)/Al_2O_3†	1%CO_2+10%O_2/N_2	100%H_2	0.14	450	[4]
Ca(30)-Ni(10)/Al_2O_3†	1%CO_2+10%O_2/N_2	100%H_2	0.064	450	[4]
Ni(10)/Al_2O_3	2.5%CO_2+10%O_2/N_2	100%H_2	0.43	500	[5]
Ni(10)/CaO	2.5%CO_2+10%O_2/N_2	100%H_2	20.4	500	[5]
Ni(10)-Ca(28)/Al_2O_3	2.5%CO_2+10%O_2/N_2	100%H_2	29.9	500	[5]
Ni(10)-Ca(8)/Al_2O_3	2.5%CO_2+10%O_2/N_2	100%H_2	8.66	500	[5]
Ni(10)-Ca(14)/Al_2O_3	2.5%CO_2+10%O_2/N_2	100%H_2	15.54	500	[5]
Ni(10)-Ca(32)/Al_2O_3	2.5%CO_2+10%O_2/N_2	100%H_2	24.1	500	[5]
Ni(30)-Ca(28)/Al_2O_3	2.5%CO_2+10%O_2/N_2	100%H_2	20.7	500	[5]
Ni(50)-Ca(28)/Al_2O_3	2.5%CO_2+10%O_2/N_2	100%H_2	22.63	500	[5]
Ni(10)-Ca(28)/Al_2O_3	2.5%CO_2+10%O_2/N_2	100%H_2	15.1	400	[5]
Ni(10)-Ca(28)/Al_2O_3	2.5%CO_2/10%O_2/N_2	100%H_2	5.91	300	[5]
Ni(10)-Ca(6)/Al_2O_3†	0.25%CO_2+10%O_2/N_2	100%H_2	14.0	350	[6]
Ni_2Ca_2-Mg_2Al_2 /LDH	10%CO_2+5%O_2/He	20%H_2/He	15.68	320	[7]
Ni_2Ca_4-Al_2/LDH	10%CO_2+5%O_2/He	20%H_2/He	12.88	320	[7]

Ni_2Mg_2-Al_2-/LDH	10%CO_2+5%O_2/He	20%H_2/He	6.72	320	[7]
Ni(30)/CaO(15)-MgO(15)-Al_2O_3	10%CO_2+5%O_2/He	20%H_2/He	6.16	320	[7]
Ru(0.84)-Ba(16)/Al_2O_3	1%CO_2+3%O_2+2.5%H_2O/He	4%H_2/He	1.12	350	[8]
Ru(1)/Al_2O_3 + Ba(16)/Al_2O_3	1%CO_2+3%O_2+2.5%H_2O/He	4%H_2/He	0.63	350	[8]
Na-Ni/Al_2O_3	5%CO_2+4.5%O_2+11%H_2O/Ar	5%H_2/Ar	0.47	350	[9]
K-Ni/Al_2O_3	5%CO_2+11%H_2O+4.5%O_2/Ar	5%H_2/Ar	2.333	350	[9]
Ba-Ni/Al_2O_3	5%CO_2+11%H_2O+4.5%O_2/Ar	5%H_2/Ar	0.093	350	[9]
Ru(0.5)-Na_2O(6.1) /Al_2O_3	7.5%CO_2+4.5%O_2 +15%H_2O/N_2	15%H_2/N_2	13.44	320	[10]
Ru(1)-Na_2O(6.1) /Al_2O_3	7.5%CO_2+4.5%O_2 +15%H_2O/N_2	15%H_2/N_2	14.93	320	[10]
Ru(1)-Na/Al_2O_3	10%CO_2+10%O_2 +10%H_2O/He	10%H_2/Ar	2.6	300	[11]
Ru(1)-Na/Al_2O_3	10%CO_2+10%O_2/He	10%H_2/Ar	15.4	300	[11]
Ru(1)-Na/Al_2O_3	10%CO_2+10%O_2/He	10%H_2/Ar	24.3	300	[11]
HT-23NiR	7.5%CO_2+4.5%O_2/He	100%H_2	0.020	250	[12]
HT-23NiR	7.5%CO_2+4.5%O_2/He	100%H_2	0.028	300	[12]
HT-23NiR	7.5%CO_2+4.5%O_2/He	100%H_2	0.022	320	[12]
HT-46NiR	7.5%CO_2+4.5%O_2/He	100%H_2	0.032	250	[12]
HT-46NiR	7.5%CO_2+4.5%O_2/He	100%H_2	0.038	300	[12]
HT-46NiR	7.5%CO_2+4.5%O_2/He	100%H_2	0.032	320	[12]
Ni-Pr/CeO_2	10%CO_2+10%O_2/Ar	10%H_2/Ar	3.11	300	[13]
RuNi-Pr/CeO_2	10%CO_2+10%O_2/Ar	10%H_2/Ar	3.70	300	[13]

*This study, † using Fig. 2b system.

Table S2. Summary of the reported CO_2 capture and methanation. Entries without *, †, or ‡ symbols using Fig. 1a system.

DFMs or catalyst	CO_2 capture gas	Hydrogenation gas	CH_4 yield [%]	*T* [°C]	ref
Ru(5)-Na_2CO_3(10)/Al_2O_3	5%CO_2/N_2	5%H_2/N_2	5.23	320	14
Ru(5)-K_2CO_3(10)/Al_2O_3	5%CO_2/N_2	5%H_2/N_2	4.53	320	14
Ni(1)/$CeCaCO_3$	15%CO_2/N_2	100%H_2	8.96	550	15
Ni(10)/CaO	15%CO_2/N_2	100%H_2	3.73	550	15
Ni(1)/CeO_2-CaOphy	15%CO_2/N_2	100%H_2	11.9	550	15
Ni(10)/g-Al_2O_3	5%CO_2/N_2	100%H_2	0.19	450	16
Ni(10)-Na(15)/g-Al_2O_3	5%CO_2/N_2	100%H_2	3.33	450	16
Ni(10)-K(15)/g-Al_2O_3	5%CO_2/N_2	100%H_2	2.51	450	16
Ni(10)-Ca(15)/g-Al_2O_3	5%CO_2/N_2	100%H_2	1.08	450	16
Ni(10)-Na(15)/g-Al_2O_3	5%CO_2/N_2	100%H_2	4.77	450	16
Ni(10)-Na(15)/g-Al_2O_3	0.04%CO_2/N_2	100%H_2	17.8	450	16
Ni(10)-Na(15)/g-Al_2O_3	0.01%CO_2/N_2	100%H_2	49.7	450	16
Ni(10)-Na(15)/g-Al_2O_3‡	2%CO_2/N_2	100%H_2	99	400	17
Ru(10)/CaO	1.4%CO_2/Ar	10%H_2/Ar	31.1	370	18
Ru(10)/Na_2CO_3	1.4%CO_2/Ar	10%H_2/Ar	48.9	370	18
Ru(5)/CaO	11%CO_2/Ar	10%H_2/Ar	2.04	280	18
Ru(5)/CaO	11%CO_2/Ar	10%H_2/Ar	1.95	310	18
Ru(5)/CaO	11%CO_2/Ar	10%H_2/Ar	1.87	340	18
Ru(5)/CaO	11%CO_2/Ar	10%H_2/Ar	1.70	370	18
Ru(5)/CaO	11%CO_2/Ar	10%H_2/Ar	1.53	400	18
Ru(10)/CaO	11%CO_2/Ar	10%H_2/Ar	3.39	280	18
Ru(10)/CaO	11%CO_2/Ar	10%H_2/Ar	3.56	310	18
Ru(10)/CaO	11%CO_2/Ar	10%H_2/Ar	3.73	340	18
Ru(10)/CaO	11%CO_2/Ar	10%H_2/Ar	3.90	370	18
Ru(10)/CaO	11%CO_2/Ar	10%H_2/Ar	4.07	400	18
Ru(15)/CaO	11%CO_2/Ar	10%H_2/Ar	3.05	280	18
Ru(15)/CaO	11%CO_2/Ar	10%H_2/Ar	4.50	310	18
Ru(15)/CaO	11%CO_2/Ar	10%H_2/Ar	5.43	340	18
Ru(15)/CaO	11%CO_2/Ar	10%H_2/Ar	6.11	370	18
Ru(15)/CaO	11%CO_2/Ar	10%H_2/Ar	6.45	400	18
Ru(5)/Na_2CO_3	11%CO_2/Ar	10%H_2/Ar	2.55	280	18
Ru(5)/Na_2CO_3	11%CO_2/Ar	10%H_2/Ar	2.21	310	18
Ru(5)/Na_2CO_3	11%CO_2/Ar	10%H_2/Ar	1.87	340	18
Ru(5)/Na_2CO_3	11%CO_2/Ar	10%H_2/Ar	1.70	370	18

Ru(5)/Na_2CO_3	11%CO_2/Ar	10%H_2/Ar	1.53	400	[18]
Ru(10)/Na_2CO_3	11%CO_2/Ar	10%H_2/Ar	6.11	280	[18]
Ru(10)/Na_2CO_3	11%CO_2/Ar	10%H_2/Ar	6.19	310	[18]
Ru(10)/Na_2CO_3	11%CO_2/Ar	10%H_2/Ar	6.11	340	[18]
Ru(10)/Na_2CO_3	11%CO_2/Ar	10%H_2/Ar	5.85	370	[18]
Ru(10)/Na_2CO_3	11%CO_2/Ar	10%H_2/Ar	5.18	400	[18]
Ru(15)/Na_2CO_3	11%CO_2/Ar	10%H_2/Ar	5.77	280	[18]
Ru(15)/Na_2CO_3	11%CO_2/Ar	10%H_2/Ar	6.11	310	[18]
Ru(15)/Na_2CO_3	11%CO_2/Ar	10%H_2/Ar	6.11	340	[18]
Ru(15)/Na_2CO_3	11%CO_2/Ar	10%H_2/Ar	6.02	370	[18]
Ru(15)/Na_2CO_3	11%CO_2/Ar	10%H_2/Ar	5.85	400	[18]
Ni(5)-CaO(15)/Al_2O_3	10%CO_2/Ar	10%H_2/Ar	1.70	520	[19]
Ni(10)-CaO(15)/Al_2O_3	10%CO_2/Ar	10%H_2/Ar	1.96	520	[19]
Ni(10)-CaO(15)/Al_2O_3 coimp	10%CO_2/Ar	10%H_2/Ar	2.05	520	[19]
Ni(15)-CaO(15)/Al_2O_3	10%CO_2/Ar	10%H_2/Ar	2.65	520	[19]
Ni(5)-CaO(15)/Al_2O_3	10%CO_2/Ar	10%H_2/Ar	1.31	480	[19]
Ni(10)-CaO(15)/Al_2O_3	10%CO_2/Ar	10%H_2/Ar	1.90	480	[19]
Ni(10)-CaO(15)/Al_2O_3 coimp	10%CO_2/Ar	10%H_2/Ar	1.87	480	[19]
Ni(15)-CaO(15)/Al_2O_3	10%CO_2/Ar	10%H_2/Ar	2.43	480	[19]
Ni(5)-CaO(15)/Al_2O_3	10%CO_2/Ar	10%H_2/Ar	1.4	440	[19]
Ni(10)-CaO(15)/Al_2O_3	10%CO_2/Ar	10%H_2/Ar	1.50	440	[19]
Ni(10)-CaO(15)/Al_2O_3 coimp	10%CO_2/Ar	10%H_2/Ar	1.50	440	[19]
Ni(15)-CaO(15)/Al_2O_3	10%CO_2/Ar	10%H_2/Ar	2.33	440	[19]
Ni(5)-CaO(15)/Al_2O_3	10%CO_2/Ar	10%H_2/Ar	1.4	400	[19]
Ni(10)-CaO(15)/Al_2O_3	10%CO_2/Ar	10%H_2/Ar	1.49	400	[19]
Ni(10)-CaO(15)/Al_2O_3 coimp	10%CO_2/Ar	10%H_2/Ar	1.31	400	[19]
Ni(15)-CaO(15)/Al_2O_3	10%CO_2/Ar	10%H_2/Ar	2.24	400	[19]
Ni(5)-CaO(15)/Al_2O_3	10%CO_2/Ar	10%H_2/Ar	1.31	360	[19]
Ni(10)-CaO(15)/Al_2O_3	10%CO_2/Ar	10%H_2/Ar	1.4	360	[19]
Ni(10)-CaO(15)/Al_2O_3 coimp	10%CO_2/Ar	10%H_2/Ar	0.93	360	[19]
Ni(15)-CaO(15)/Al_2O_3	10%CO_2/Ar	10%H_2/Ar	2.05	360	[19]
Ni(5)-CaO(15)/Al_2O_3	10%CO_2/Ar	10%H_2/Ar	0.93	320	[19]
Ni(10)-CaO(15)/Al_2O_3	10%CO_2/Ar	10%H_2/Ar	1.12	320	[19]
Ni(10)-CaO(15)/Al_2O_3 coimp	10%CO_2/Ar	10%H_2/Ar	0.47	320	[19]
Ni(15)-CaO(15)/Al_2O_3	10%CO_2/Ar	10%H_2/Ar	1.49	320	[19]
Ni(5)-CaO(15)/Al_2O_3	10%CO_2/Ar	10%H_2/Ar	0.19	280	[19]
Ni(10)-CaO(15)/Al_2O_3	10%CO_2/Ar	10%H_2/Ar	0.56	280	[19]
Ni(10)-CaO(15)/Al_2O_3 coimp	10%CO_2/Ar	10%H_2/Ar	0.19	280	[19]

Ni(15)-CaO(15)/Al_2O_3	10%CO_2/Ar	10%H_2/Ar	0.93	280	[19]
Ni(5)-Na_2CO_3(10)/Al_2O_3	10%CO_2/Ar	10%H_2/Ar	1.87	520	[19]
Ni(10)-Na_2CO_3(10)/Al_2O_3	10%CO_2/Ar	10%H_2/Ar	1.96	520	[19]
Ni(10)-Na_2CO_3(10)/Al_2O_3 coimp	10%CO_2/Ar	10%H_2/Ar	1.96	520	[19]
Ni(15)-Na_2CO_3(10)/Al_2O_3	10%CO_2/Ar	10%H_2/Ar	2.05	520	[19]
Ni(5)-Na_2CO_3(10)/Al_2O_3	10%CO_2/Ar	10%H_2/Ar	2.24	480	[19]
Ni(10)-Na_2CO_3(10)/Al_2O_3	10%CO_2/Ar	10%H_2/Ar	2.61	480	[19]
Ni(10)-Na_2CO_3(10)/Al_2O_3 coimp	10%CO_2/Ar	10%H_2/Ar	2.52	480	[19]
Ni(15)-Na_2CO_3(10)/Al_2O_3	10%CO_2/Ar	10%H_2/Ar	2.52	480	[19]
Ni(5)-Na_2CO_3(10)/Al_2O_3	10%CO_2/Ar	10%H_2/Ar	2.33	440	[19]
Ni(10)-Na_2CO_3(10)/Al_2O_3	10%CO_2/Ar	10%H_2/Ar	2.8	440	[19]
Ni(10)-Na_2CO_3(10)/Al_2O_3 coimp	10%CO_2/Ar	10%H_2/Ar	2.8	440	[19]
Ni(15)-Na_2CO_3(10)/Al_2O_3	10%CO_2/Ar	10%H_2/Ar	2.8	440	[19]
Ni(5)-Na_2CO_3(10)/Al_2O_3	10%CO_2/Ar	10%H_2/Ar	2.8	400	[19]
Ni(10)-Na_2CO_3(10)/Al_2O_3	10%CO_2/Ar	10%H_2/Ar	3.45	400	[19]
Ni(10)-Na_2CO_3(10)/Al_2O_3 coimp	10%CO_2/Ar	10%H_2/Ar	3.43	400	[19]
Ni(15)-Na_2CO_3(10)/Al_2O_3	10%CO_2/Ar	10%H_2/Ar	3.47	400	[19]
Ni(5)-Na_2CO_3(10)/Al_2O_3	10%CO_2/Ar	10%H_2/Ar	3.36	360	[19]
Ni(10)-Na_2CO_3(10)/Al_2O_3	10%CO_2/Ar	10%H_2/Ar	3.17	360	[19]
Ni(10)-Na_2CO_3(10)/Al_2O_3 coimp	10%CO_2/Ar	10%H_2/Ar	2.8	360	[19]
Ni(15)-Na_2CO_3(10)/Al_2O_3	10%CO_2/Ar	10%H_2/Ar	3.27	360	[19]
Ni(5)-Na_2CO_3(10)/Al_2O_3	10%CO_2/Ar	10%H_2/Ar	1.4	320	[19]
Ni(10)-Na_2CO_3(10)/Al_2O_3	10%CO_2/Ar	10%H_2/Ar	2.05	320	[19]
Ni(10)-Na_2CO_3(10)/Al_2O_3 coimp	10%CO_2/Ar	10%H_2/Ar	1.49	320	[19]
Ni(15)-Na_2CO_3(10)/Al_2O_3	10%CO_2/Ar	10%H_2/Ar	2.33	320	[19]
Ni(5)-Na_2CO_3(10)/Al_2O_3	10%CO_2/Ar	10%H_2/Ar	0.093	280	[19]
Ni(10)-Na_2CO_3(10)/Al_2O_3	10%CO_2/Ar	10%H_2/Ar	0.56	280	[19]
Ni(10)-Na_2CO_3(10)/Al_2O_3 coimp	10%CO_2/Ar	10%H_2/Ar	0.37	280	[19]
Ni(15)-Na_2CO_3(10)/Al_2O_3	10%CO_2/Ar	10%H_2/Ar	0.65	280	[19]
Ru(2.5)/CeO_2	65%CO_2/N_2	5%H_2/N_2	2.96	300	[20]
Ru(5)/CeO_2	65%CO_2/N_2	5%H_2/N_2	3.41	300	[20]
Ru(10)/CeO_2	65%CO_2/N_2	5%H_2/N_2	3.65	300	[20]
Ni(20)/MgO	10%CO_2/Ar	5%H_2/Ar	0.17	250	[21]
Ni(20)/MgO	10%CO_2/Ar	5%H_2/Ar	0.50	300	[21]
Ni(20)/MgO	10%CO_2/Ar	5%H_2/Ar	0.45	350	[21]
Ni(50)/MgO	10%CO_2/Ar	5%H_2/Ar	0.34	250	[21]
Ni(50)/MgO	10%CO_2/Ar	5%H_2/Ar	1.23	300	[21]
Ni(50)/MgO	10%CO_2/Ar	5%H_2/Ar	1.06	350	[21]

Ni(80)/MgO	10%CO_2/Ar	5%H_2/Ar	0.45	250	[21]
Ni(80)/MgO	10%CO_2/Ar	5%H_2/Ar	1.51	300	[21]
Ni(80)/MgO	10%CO_2/Ar	5%H_2/Ar	1.29	350	[21]
Com-Ni(50)/MgO	10%CO_2/Ar	5%H_2/Ar	0.017	250	[21]
Com-Ni(50)/MgO	10%CO_2/Ar	5%H_2/Ar	0.45	300	[21]
Com-Ni(50)/MgO	10%CO_2/Ar	5%H_2/Ar	0.039	350	[21]
Ni/CaO	10%CO_2/N_2	10%H_2/N_2	0.67	400	[22]
Ni/CaO-MgO	10%CO_2/N_2	10%H_2/N_2	0.69	400	[22]
Ni/CaO-MgO	10%CO_2/N_2	10%H_2/N_2	0.24	400	[22]
Ni/MgO	10%CO_2/N_2	10%H_2/N_2	0.15	400	[22]
AMS-Ni/MgO	65%CO_2/N_2	20%H_2/N_2	0.040	450	[23]
AMS-Ni/MgO	65%CO_2/N_2	60%H_2/N_2	0.052	450	[23]
AMS-Ni/MgO	65%CO_2/N_2	100%H_2	0.046	450	[23]
AMS-Ni/MgO	65%CO_2/N_2	100%H_2	0.034	400	[23]
AMS-Ni/MgO	65%CO_2/N_2	100%H_2	0.044	500	[23]
Ru(0.84)-Ba(16)/Al_2O_3	1%CO_2/He	4%H_2/He	2.06	350	[24]
Ru(1)/Al_2O_3 + Ba(16)/Al_2O_3	1%CO_2/He	4%H_2/He	1.32	350	[24]
Ru(1)/Al_2O_3	1%CO_2/He	4%H_2/He	0.027	350	[3]
Ru(0.99)-Li(1)/Al_2O_3	1%CO_2/He	4%H_2/He	0.027	350	[3]
Ru(0.97)-Na(3)/Al_2O_3	1%CO_2/He	4%H_2/He	0.63	350	[3]
Ru(0.95)-K(5)/Al_2O_3	1%CO_2/He	4%H_2/He	2.53	350	[3]
Ru(0.97)-Mg(3.2)/Al_2O_3	1%CO_2/He	4%H_2/He	0.054	350	[3]
Ru(0.95)-Ca(5.1)/Al_2O_3	1%CO_2/He	4%H_2/He	1.85	350	[3]
Ru(0.84)-Ba(16)/Al_2O_3	1%CO_2/He	4%H_2/He	3.02	350	[3]
Ru/rod-CeO_2-MgO	35%CO_2/N_2	5%H_2/N_2	0.22	300	[25]
Ru/particle-CeO_2-MgO	35%CO_2/N_2	5%H_2/N_2	0.24	300	[25]
Ru/cube-CeO_2-MgO	35%CO_2/N_2	5%H_2/N_2	0.032	300	[25]
Ni-Na_2CO_3/Al_2O_3	9.5%CO_2/N_2	10%H_2/N_2	1.12	320	[26]
Ni-CaO/Al_2O_3	9.5%CO_2/N_2	10%H_2/N_2	0.88	320	[26]
Li_4SiO_4@Ni(2.5)/CeO_2	15%CO_2/N_2	100%H_2	9.16	560	[27]
Li_4SiO_4@Ni(5)/CeO_2	15%CO_2/N_2	100%H_2	9.96	560	[27]
Li_4SiO_4@Ni(7.5)/CeO_2	15%CO_2/N_2	100%H_2	9.56	560	[27]
Na-Ni/Al_2O_3	5%CO_2/Ar	5%H_2/Ar	0.16	250	[28]
K-Ni/Al_2O_3	5%CO_2/Ar	5%H_2/Ar	0.17	250	[28]
Ba-Ni/Al_2O_3	5%CO_2/Ar	5%H_2/Ar	0.084	250	[28]
Na-Ni/Al_2O_3	5%CO_2/Ar	5%H_2/Ar	1.87	300	[28]
K-Ni/Al_2O_3	5%CO_2/Ar	5%H_2/Ar	2.43	300	[28]

Ba-Ni/Al_2O_3	5%CO_2/Ar	5%H_2/Ar	0.47	300	[28]
Ni/Al_2O_3	5%CO_2/Ar	5%H_2/Ar	0.47	300	[28]
Na-Ni/Al_2O_3	5%CO_2/Ar	5%H_2/Ar	3.17	350	[28]
K-Ni/Al_2O_3	5%CO_2/Ar	5%H_2/Ar	1.49	350	[28]
Ba-Ni/Al_2O_3	5%CO_2/Ar	5%H_2/Ar	0.93	350	[28]
Na-Ni/Al_2O_3	5%CO_2/Ar	5%H_2/Ar	2.61	400	[28]
K-Ni/Al_2O_3	5%CO_2/Ar	5%H_2/Ar	1.59	400	[28]
Ba-Ni/Al_2O_3	5%CO_2/Ar	5%H_2/Ar	0.75	400	[28]
Na-Ni/Al_2O_3	5%CO_2/Ar	5%H_2/Ar	2.89	450	[28]
K-Ni/Al_2O_3	5%CO_2/Ar	5%H_2/Ar	2.29	450	[28]
Ba-Ni/Al_2O_3	5%CO_2/Ar	5%H_2/Ar	0.65	450	[28]
Ru(0.89)-Li(5)/Al_2O_3	10%CO_2/N_2	10%H_2/N_2	2.02	280	[29]
Ru(3)-K(10)/Al_2O_3	5%CO_2/Ar	5%H_2/Ar	4.85	300	[29]
Ru(3)-K(10)/Al_2O_3	5%CO_2/Ar	5%H_2/Ar	0.93	350	[29]
Ru(3)-K(10)/Al_2O_3	5%CO_2/Ar	5%H_2/Ar	7.09	400	[29]
Ru(3)-K(10)/Al_2O_3	5%CO_2/Ar	5%H_2/Ar	4.57	450	[29]
Ru(3)-Na(10)/Al_2O_3	5%CO_2/Ar	5%H_2/Ar	10.4	300	[29]
Ru(3)-Na(10)/Al_2O_3	5%CO_2/Ar	5%H_2/Ar	9.15	350	[29]
Ru(3)-Na(10)/Al_2O_3	5%CO_2/Ar	5%H_2/Ar	7.65	400	[29]
Ru(3)-Na(10)/Al_2O_3	5%CO_2/Ar	5%H_2/Ar	3.45	450	[29]
Ru(3)-Ba(10)/Al_2O_3	5%CO_2/Ar	5%H_2/Ar	1.49	250	[29]
Ru(3)-Ba(10)/Al_2O_3	5%CO_2/Ar	5%H_2/Ar	6.35	300	[29]
Ru(3)-Ba(10)/Al_2O_3	5%CO_2/Ar	5%H_2/Ar	4.85	350	[29]
Ru(3)-Ba(10)/Al_2O_3	5%CO_2/Ar	5%H_2/Ar	2.05	400	[29]
Ru(3)-Ba(10)/Al_2O_3	5%CO_2/Ar	5%H_2/Ar	2.61	450	[29]
Ru(1)-Na(20)/Al_2O_3	10%CO_2/N_2	5%H_2/N_2	1.53	340	[30]
Ru(0.5)-Na_2O(6.1) /Al_2O_3	7.5%CO_2/N_2	15%H_2/N_2	9.71	320	[31]
Ru(0.5)-Na_2O(6.1)/Al_2O_3	7.5%CO_2+ 15%H_2O/N_2	15%H_2/N_2	7.47	320	[31]
Ni/Hydrotalcite	15%CO_2/N_2	100%H_2	3.88	400	[32]
Ni/Hydrotalcite	15%CO_2/N_2	100%H_2	4.85	450	[32]
Ni/Hydrotalcite	15%CO_2/N_2	100%H_2	4.78	500	[32]
Ni/Hydrotalcite	15%CO_2/N_2	100%H_2	3.96	550	[32]
Ni/Hydrotalcite	15%CO_2/N_2	100%H_2	3.58	600	[32]
Ni-Cs(10)/Hydrotalcite	15%CO_2/N_2	100%H_2	4.93	350	[32]
Ni(1)/CaO	15%CO_2/N_2	100%H_2	2.99	550	[33]
Ni(10)/CaO	15%CO_2/N_2	100%H_2	3.73	550	[33]
Ni(1)/CeCaO	15%CO_2/N_2	100%H_2	4.93	550	[33]

Ni(1)/CeCaCO3	15%CO_2/N_2	100%H_2	8.96	550	33
Ni(1)/CeO_2 + CaO	15%CO_2/N_2	100%H_2	11.95	550	33
$LaNiO_3$(20)/CeO_2	10%CO_2/Ar	5%H_2/Ar	1.16	280	34
$LaNiO_3$(20)/CeO_2	10%CO_2/Ar	5%H_2/Ar	1.77	320	34
$LaNiO_3$(20)/CeO_2	10%CO_2/Ar	5%H_2/Ar	1.87	360	34
$LaNiO_3$(20)/CeO_2	10%CO_2/Ar	5%H_2/Ar	2.02	400	34
$LaNiO_3$(20)/CeO_2	10%CO_2/Ar	5%H_2/Ar	2.05	440	34
$LaNiO_3$(20)/CeO_2	10%CO_2/Ar	5%H_2/Ar	2.00	480	34
$LaNiO_3$(20)/CeO_2	10%CO_2/Ar	5%H_2/Ar	1.92	520	34
$La_{0.7}Ca_{0.3}NiO_3$(20)/CeO_2	10%CO_2/Ar	5%H_2/Ar	1.4	280	34
$La_{0.7}Ca_{0.3}NiO_3$(20)/CeO_2	10%CO_2/Ar	5%H_2/Ar	1.87	320	34
$La_{0.7}Ca_{0.3}NiO_3$(20)/CeO_2	10%CO_2/Ar	5%H_2/Ar	2.24	360	34
$La_{0.7}Ca_{0.3}NiO_3$(20)/CeO_2	10%CO_2/Ar	5%H_2/Ar	2.39	400	34
$La_{0.7}Ca_{0.3}NiO_3$(20)/CeO_2	10%CO_2/Ar	5%H_2/Ar	2.61	440	34
$La_{0.7}Ca_{0.3}NiO_3$(20)/CeO_2	10%CO_2/Ar	5%H_2/Ar	2.8	480	34
$La_{0.7}Ca_{0.3}NiO_3$(20)/CeO_2	10%CO_2/Ar	5%H_2/Ar	2.37	520	34
$La_{0.7}Ba_{0.3}NiO_3$(20)/CeO_2	10%CO_2/Ar	5%H_2/Ar	1.16	280	34
$La_{0.7}Ba_{0.3}NiO_3$(20)/CeO_2	10%CO_2/Ar	5%H_2/Ar	1.77	320	34
$La_{0.7}Ba_{0.3}NiO_3$(20)/CeO_2	10%CO_2/Ar	5%H_2/Ar	2.02	360	34
$La_{0.7}Ba_{0.3}NiO_3$(20)/CeO_2	10%CO_2/Ar	5%H_2/Ar	2.05	400	34
$La_{0.7}Ba_{0.3}NiO_3$(20)/CeO_2	10%CO_2/Ar	5%H_2/Ar	1.98	440	34
$La_{0.7}Ba_{0.3}NiO_3$(20)/CeO_2	10%CO_2/Ar	5%H_2/Ar	1.59	480	34
$La_{0.7}Ba_{0.3}NiO_3$(20)/CeO_2	10%CO_2/Ar	5%H_2/Ar	1.4	520	34
$La_{0.7}Na_{0.3}NiO_3$(20)/CeO_2	10%CO_2/Ar	5%H_2/Ar	1.08	280	34
$La_{0.7}Na_{0.3}NiO_3$(20)/CeO_2	10%CO_2/Ar	5%H_2/Ar	1.21	320	34
$La_{0.7}Na_{0.3}NiO_3$(20)/CeO_2	10%CO_2/Ar	5%H_2/Ar	1.30	360	34
$La_{0.7}Na_{0.3}NiO_3$(20)/CeO_2	10%CO_2/Ar	5%H_2/Ar	1.16	400	34
$La_{0.7}Na_{0.3}NiO_3$(20)/CeO_2	10%CO_2/Ar	5%H_2/Ar	1.10	440	34
$La_{0.7}Na_{0.3}NiO_3$(20)/CeO_2	10%CO_2/Ar	5%H_2/Ar	1.03	480	34
$La_{0.7}Na_{0.3}NiO_3$(20)/CeO_2	10%CO_2/Ar	5%H_2/Ar	0.75	520	34
$La_{0.7}K_{0.3}NiO_3$(20)/CeO_2	10%CO_2/Ar	5%H_2/Ar	0.65	280	34
$La_{0.7}K_{0.3}NiO_3$(20)/CeO_2	10%CO_2/Ar	5%H_2/Ar	0.896	320	34
$La_{0.7}K_{0.3}NiO_3$(20)/CeO_2	10%CO_2/Ar	5%H_2/Ar	0.93	360	34
$La_{0.7}K_{0.3}NiO_3$(20)/CeO_2	10%CO_2/Ar	5%H_2/Ar	0.93	400	34
$La_{0.7}K_{0.3}NiO_3$(20)/CeO_2	10%CO_2/Ar	5%H_2/Ar	0.91	440	34
$La_{0.7}K_{0.3}NiO_3$(20)/CeO_2	10%CO_2/Ar	5%H_2/Ar	0.90	480	34
$La_{0.7}K_{0.3}NiO_3$(20)/CeO_2	10%CO_2/Ar	5%H_2/Ar	0.84	520	34

Ru/CeO_2-$CaCO_3$	20%CO_2/N_2	100%H_2	1.79	350	[35]
Ru/CeO_2-KNO_3 $CaCO_3$	20%CO_2/N_2	100%H_2	2.52	350	[35]
Ru/CeO_2-$LiNO_3$ $CaCO_3$	20%CO_2/N_2	100%H_2	1.456	350	[35]
Ru/CeO_2-(Li-K)NO_3 $CaCO_3$	20%CO_2/N_2	100%H_2	2.184	350	[35]
Ru/CeO_2-KNO_3 $CaCO_3$	20%CO_2/N_2	100%H_2	3.192	400	[35]
Ru/CeO_2-KNO_3 $CaCO_3$	20%CO_2/N_2	100%H_2	5.32	450	[35]
Ru/CeO_2-KNO_3 $CaCO_3$	20%CO_2/N_2	100%H_2	3.81	500	[35]
Ru(0.25)-Na/Al_2O_3	10%CO_2/Ar	10%H_2/Ar	0.72	300	[36]
Ru(0.5)-Na/Al_2O_3	10%CO_2/Ar	10%H_2/Ar	2.27	300	[36]
Ru(1)-Na/Al_2O_3	10%CO_2/Ar	10%H_2/Ar	2.688	300	[36]
Ru(2)-Na/Al_2O_3	10%CO_2/Ar	10%H_2/Ar	2.68	300	[36]
Ru(4)-Na/Al_2O_3	10%CO_2/Ar	10%H_2/Ar	2.66	300	[36]
Ni-Pr/CeO_2	10%CO_2/Ar	10%H_2/Ar	4.66	300	[13]
RuNi-Pr/CeO_2	10%CO_2/Ar	10%H_2/Ar	5.62	300	[13]
Ni/MgO	65%CO_2/N_2	50%H_2/N_2	0.046	500	[37]

‡ using a circulating fluidized system similar to Fig. 2b

Table S3. Summary of the continuous CO_2 capture and RWGS reaction in this study and other reported CO_2 capture and RWGS reaction considering the effect of coexistent O_2. Entries without *, †, or ‡ symbols using Fig. 1a system.

DFMs or catalyst	CO_2 capture gas	Hydrogenation gas	CO yield [%]	*T* [°C]	ref
$Cu/ZnO/Al_2O_3$*	$10\%CO_2+10\%O_2/He$	$100\%H_2$	85.1	650	*
Pt(1)-Na(3)/Al_2O_3	$1\%CO_2+10\%O_2/N_2$	$5\%H_2/N_2$	8.8	350	[38]
Pt(1)-Na(3)/Al_2O_3†	$1\%CO_2+10\%O_2/N_2$	100% H_2	89.0	350	[38]
Pt(1)-Na(3)/MgO	$1\%CO_2+10\%O_2/N_2$	$5\%H_2/N_2$	3.4	350	[38]
Pt(1)-Ca(6)/Al_2O_3	$1\%CO_2+10\%O_2/N_2$	$5\%H_2/N_2$	2.3	350	[38]
Pt(1)-Mg(3)/Al_2O_3	$1\%CO_2/10\%O_2/N_2$	$5\%H_2/N_2$	0.56	350	[38]
Pt(1)-K(6)/Al_2O_3	$1\%CO_2+10\%O_2/N_2$	$5\%H_2/N_2$	0.39	350	[38]
Ru(1)-Na(3)/Al_2O_3	$1\%CO_2+10\%O_2/N_2$	$5\%H_2/N_2$	0.34	350	[38]
Cu(1)-Na(3)/Al_2O_3	$1\%CO_2+10\%O_2/N_2$	$5\%H_2/N_2$	0.17	350	[38]
Pt(1)-Na(3)/SiO_2	$1\%CO_2+10\%O_2/N_2$	$5\%H_2/N_2$	0.34	350	[38]
Pt(1)-Na(3)/TiO_2	$1\%CO_2+10\%O_2/N_2$	$5\%H_2/N_2$	1.68	350	[38]
Rb-Ni/Al_2O_3†	$0.5\%CO_2+10\%O_2/N_2$	$20\%H_2/N_2$	47.8	450	[39]
Pt-Na/Al_2O_3†	$0.5\%CO_2+10\%O_2/N_2$	$20\%H_2/N_2$	34.7	450	[39]
Ni-Rb/Al_2O_3†	$0.5\%CO_2+10\%O_2/N_2$	$20\%H_2/N_2$	28.2	450	[39]
Na-Ni/Al_2O_3†	$0.5\%CO_2+10\%O_2/N_2$	$20\%H_2/N_2$	12.9	450	[39]
Mg-Ni/Al_2O_3†	$0.5\%CO_2+10\%O_2/N_2$	$20\%H_2/N_2$	0.54	450	[39]
Na/Al_2O_3	$0.5\%CO_2+10\%O_2/N_2$	$20\%H_2/N_2$	15.1	450	[39]
Rb/Al_2O_3	$0.5\%CO_2+10\%O_2/N_2$	$20\%H_2/N_2$	16.1	450	[39]
Fe(6.91)Cr(0.58)Cu(0.20)-K(9.98)/hydrotalcite	$5.8\%CO_2+5\%O_2+4\%H_2O/N_2$	$100\%H_2$	41.3	450	[40]
Fe(6.91)Cr(0.58)Cu(0.20)-K(9.98)/hydrotalcite	$5.8\%CO_2+5\%O_2+4\%H_2O/N_2$	$100\%H_2$	52.2	500	[40]
Fe(6.91)Cr(0.58)Cu(0.20)-K(9.98)/hydrotalcite	$5.8\%CO_2+5\%O_2+4\%H_2O/N_2$	$100\%H_2$	56.0	530	[40]

*This study † using Fig. 2b system.

Table S4. Summary of reported CO_2 capture and RWGS reaction. Entries without *, †, or ‡ symbols using Fig. 1a system.

DFMs or catalyst	CO_2 capture gas	Hydrogenation gas	CO yield. [%]	*T* [°C]	ref
$Ca_1Ni_{0.1}O$	15%CO_2/N_2	5%H_2/N_2	10.3	650	[41]
$Ca_1Ni_{0.1}Ce_{0.017}O$	15%CO_2/N_2	5%H_2/N_2	10.8	650	[41]
$Ca_1Ni_{0.1}Ce_{0.033}O$	15%CO_2/N_2	5%H_2/N_2	10.9	650	[41]
Fe(5)Co(5)Mg(10)/CaO	10%CO_2/He	100%H_2	30.9	650	[42]
CaO	10%CO_2/He	100%H_2	10.3	650	[42]
Fe(10)Mg(10)/CaO	10%CO_2/He	100%H_2	26.9	650	[42]
Fe(8)Co(2)Mg(10)CaO	10%CO_2/He	100%H_2	26.5	650	[42]
Fe(7.5)Co(2.5)Mg(10)CaO	10%CO_2/He	100%H_2	27.7	650	[42]
Fe(6.7)Co(3.3)Mg(10)CaO	10%CO_2/He	100%H_2	29.7	650	[42]
Fe(3.3)Co(6.7)Mg(10)CaO	10%CO_2/He	100%H_2	26.0	650	[42]
Co(10)Mg(10)CaO	10%CO_2/He	100%H_2	24.4	650	[42]
Ni(10)/CaO	10%CO_2/N_2	5%H_2/N_2	10.6	650	[43]
Ni(10)/Carbide slag(CS)	10%CO_2/N_2	5%H_2/N_2	10.6	650	[43]
Rb-Ni/Al_2O_3	0.5%CO_2/N_2	20%H_2/N_2	22.0	450	[39]
Ni(10)/CaZr(O)	15%CO_2/N_2	66.7%H_2/N_2	4.80	600	[44]
Ni(10)/CaAl(O)	15%CO_2/N_2	66.7%H_2/N_2	6.95	600	[44]
Ni(10)/CaO	15%CO_2/N_2	66.7%H_2/N_2	6.09	600	[44]
Ni(10)/CaMg(O)	15%CO_2/N_2	66.7%H_2/N_2	5.37	600	[44]
Cu(11)-K(10)/Al_2O_3	4.4%CO_2/He	100%H_2	27.6	450	[45]
Fe(6.91)Cr(0.58)Cu(0.20)-K(9.98)/hydrotalcite	5.8%CO_2/N_2	100%H_2	72.7	550	[40]
Fe(6.91)Cr(0.58)Cu(0.20)-K(9.98)/hydrotalcite	5.8%CO_2+4%H_2O/N_2	100%H_2	64.3	550	[40]
Fe(6.91)Cr(0.58)Cu(0.20)-K(9.98)/hydrotalcite	5.8%CO_2/4%O_2/N_2	100%H_2	50.8	550	[40]
Fe(6.91)Cr(0.58)Cu(0.20)-K(9.98)/hydrotalcite	7.6%CO_2/N_2	100%H_2	54.7	550	[40]
Fe(6.91)Cr(0.58)Cu(0.20)-K(9.98)/hydrotalcite	7.6%CO_2/4%H_2O/N_2	100%H_2	44.9	550	[40]
Fe(6.91)Cr(0.58)Cu(0.20)-K(9.98)/hydrotalcite	9.5%CO_2/N_2	100%H_2	38.7	550	[40]
Fe(6.91)Cr(0.58)Cu(0.20)-K(9.98)/hydrotalcite	9.5%CO_2/4%H_2O/N_2	100%H_2	32.4	550	[40]
Fe(6.91)Cr(0.58)Cu(0.20)-K(9.98)/hydrotalcite	5.8%CO_2/N_2	100%H_2	72.3	450	[40]
Fe(6.91)Cr(0.58)Cu(0.20)-K(9.98)/hydrotalcite	5.8%CO_2/N_2	100%H_2	72.7	470	[40]
Fe(6.91)Cr(0.58)Cu(0.20)-K(9.98)/hydrotalcite	5.8%CO_2/N_2	100%H_2	78.5	500	[40]
Fe(6.91)Cr(0.58)Cu(0.20)-K(9.98)/hydrotalcite	5.8%CO_2/N_2	100%H_2	83.1	530	[40]
Na(16)/Al_2O_3	5%CO_2/N_2	100%H_2	5.08	450	[46]

K(21)/Al_2O_3	5%CO_2/N_2	100%H_2	5.97	450	[46]
Ca(15)/Al_2O_3	5%CO_2/N_2	100%H_2	2.7	450	[46]
Al_2O_3	5%CO_2/N_2	100%H_2	0.30	450	[46]
Na(16)/Al_2O_3	5%CO_2/N_2	100%H_2	2.33	350	[46]
Na(16)/Al_2O_3	5%CO_2/N_2	100%H_2	4.928	400	[46]
Na(16)/Al_2O_3	5%CO_2/N_2	100%H_2	5.36	500	[46]
CaO	15%CO_2/N_2	15%H_2	1.58	600	[47]
CaO	15%CO_2/N_2	15%H_2	7.1	650	[47]
CaO	15%CO_2/N_2	15%H_2	19.3	700	[47]
CeO_2(33)/CaO	17%CO_2/N_2	5%H_2/N_2	2.16	650	[47]
CeO_2(33)/CaO	17%CO_2/N_2	5%H_2/N_2	0.98	600	[47]
CeO_2(33)/CaO	17%CO_2/N_2	5%H_2/N_2	3.63	700	[47]
CeO_2(33)/CaO	17%CO_2/N_2	5%H_2/N_2	1.81	750	[47]
CeO_2(10)/CaO	17%CO_2/N_2	5%H_2/N_2	0.84	600	[47]
CeO_2(10)/CaO	17%CO_2/N_2	5%H_2/N_2	3.56	650	[47]
CeO_2(10)/CaO	17%CO_2/N_2	5%H_2/N_2	4.88	700	[47]
CeO_2(10)/CaO	17%CO_2/N_2	5%H_2/N_2	2.23	750	[47]
CeO_2(16)/CaO	17%CO_2/N_2	5%H_2/N_2	0.70	600	[47]
CeO_2(16)/CaO	17%CO_2/N_2	5%H_2/N_2	2.51	650	[47]
CeO_2(16)/CaO	17%CO_2/N_2	5%H_2/N_2	4.74	700	[47]
CeO_2(16)/CaO	17%CO_2/N_2	5%H_2/N_2	2.65	750	[47]
CeO_2(50)/CaO	17%CO_2/N_2	5%H_2/N_2	0.56	600	[47]
CeO_2(50)/CaO	17%CO_2/N_2	5%H_2/N_2	2.23	650	[47]
CeO_2(50)/CaO	17%CO_2/N_2	5%H_2/N_2	2.93	700	[47]
CeO_2(50)/CaO	17%CO_2/N_2	5%H_2/N_2	0.84	750	[47]
CeO_2(67)/CaO	17%CO_2/N_2	5%H_2/N_2	0.35	600	[47]
CeO_2(67)/CaO	17%CO_2/N_2	5%H_2/N_2	1.39	650	[47]
CeO_2(67)/CaO	17%CO_2/N_2	5%H_2/N_2	1.39	700	[47]
CeO_2(67)/CaO	17%CO_2/N_2	5%H_2/N_2	0.56	750	[47]
Ni/CaO	10%CO_2/10%H_2O/N_2	10%H_2/N_2	21.5	700	[48]
La(15)-Ni(2.5)/CaO	10%CO_2/Ar	10%H_2/Ar	43.3	650	[49]
Mg(15)-Ni(2.5)/CaO	10%CO_2/Ar	10%H_2/Ar	38.8	650	[49]
Zr(15)-Ni(2.5)/CaO	10%CO_2/Ar	10%H_2/Ar	36.3	650	[49]
Ce(15)-Ni(2.5)/CaO	10%CO_2/Ar	10%H_2/Ar	41.3	650	[49]
Ni(2.5)/CaO	10%CO_2/Ar	10%H_2/Ar	31.36	650	[49]

References

1. Arellano-Treviño, M. A., Kanani, N., Jeong-Potter, C. W. & Farrauto, R. J. Bimetallic catalysts for CO_2 capture and hydrogenation at simulated flue gas conditions. *Chem. Eng. J.* **375**, (2019).
2. Arellano-Treviño, M. A., He, Z., Libby, M. C. & Farrauto, R. J. Catalysts and adsorbents for CO_2 capture and conversion with dual function materials: Limitations of Ni-containing DFMs for flue gas applications. *J. CO2 Util.* **31**, 143–151 (2019).
3. Porta, A., Matarrese, R., Visconti, C. G., Castoldi, L. & Lietti, L. Storage Material Effects on the Performance of Ru-Based CO_2 Capture and Methanation Dual Functioning Materials. *Ind Eng Chem Res* **60**, 6706–6718 (2021).
4. Li, L. *et al.* Continuous CO_2 capture and methanation over Ni-Ca/Al_2O_3 dual functional materials. *RSC Adv* **13**, 2213–2219 (2023).
5. Miyazaki, S. *et al. In Situ* Spectroscopic Study of CO_2 Capture and Methanation over Ni−Ca Based Dual Functional Materials. *Chem Asian J* (2023) e202301003.
6. Li, L. *et al.* Continuous direct air capture and methanation using combined system of membrane-based CO_2 capture and Ni-Ca based dual functional materials. *Appl Catal B* **339**, (2023).
7. Sakai, M., Imagawa, H. & Baba, N. Layered-double-hydroxide-based Ni catalyst for CO_2 capture and methanation. *Appl Catal A Gen* **647**, (2022).
8. Porta, A. *et al.* Ru-Ba synergistic effect in dual functioning materials for cyclic CO_2 capture and methanation. *Appl Catal B* **283**, (2021).
9. García-Bordejé, E., Belén Dongil, A., Conesa, J. M., Guerrero-Ruiz, A. & Rodríguez-Ramos, I. Dual functional materials based on Ni and different alkaline metals on alumina for the cyclic stepwise CO_2 capture and methanation. *Chemical Engineering Journal* **472**, (2023).
10. Jeong-Potter, C. *et al.* Aging study of low Ru loading dual function materials (DFM) for combined power plant effluent CO_2 capture and methanation. *Appl Catal B* **310**, (2022).
11. Tsiotsias, A. I. *et al.* CO_2 capture and methanation using Ru/Na_2O/Al_2O_3 dual-function materials: Effect of support synthesis method and Ru load. *J Environ Chem Eng* **12**, (2024).
12. Marin, J., Parra, P. & Rios, L. Improved Dual Function Materials for CO_2 Capture and In Situ Methanation. *Energy Technology* **12**, (2024).
13. Tsiotsias, A. I. *et al.* Integrating capture and methanation of CO_2 using physical mixtures of Na-Al_2O_3 and mono-/ bimetallic (Ru)Ni/Pr-CeO_2. *Chemical Engineering Journal* **491**, (2024).
14. Duyar, M. S., Wang, S., Arellano-Treviño, M. A. & Farrauto, R. J. CO_2 utilization with a novel dual function material (DFM) for capture and catalytic conversion to synthetic natural gas: An update. *Journal of CO2 Utilization* **15**, 65–71 (2016).
15. Sun, H. *et al.* Understanding the interaction between active sites and sorbents during the integrated carbon capture and utilization process. *Fuel* **286**, (2021).
16. Kosaka, F. *et al.* Enhanced Activity of Integrated CO_2 Capture and Reduction to CH_4 under Pressurized Conditions toward Atmospheric CO_2 Utilization. *ACS Sustain Chem Eng* **9**, 3452–3463 (2021).
17. Kosaka, F. *et al.* Direct and continuous conversion of flue gas CO_2 into green fuels using dual function materials in a circulating fluidized bed system. *Chemical Engineering Journal* **450**, (2022).
18. Bermejo-López, A., Pereda-Ayo, B., González-Marcos, J. A. & González-Velasco, J. R. Mechanism of the CO2 storage and in situ hydrogenation to CH_4. Temperature and adsorbent loading effects over Ru-CaO/Al2O3 and Ru-Na_2CO_3/Al_2O_3 catalysts. *Appl Catal B* **256**, (2019).
19. Bermejo-López, A., Pereda-Ayo, B., González-Marcos, J. A. & González-Velasco, J. R. Ni loading effects on dual function materials for capture and in-situ conversion of CO_2 to CH_4 using CaO or Na_2CO_3. *Journal of CO2 Utilization* **34**, 576–587 (2019).
20. Sun, H., Zhang, Y., Guan, S., Huang, J. & Wu, C. Direct and highly selective conversion of captured CO_2 into methane through integrated carbon capture and utilization over dual functional materials. *Journal of*

CO2 Utilization **38**, 262–272 (2020).
21. Guo, Z. K. *et al.* Mechanochemical synthesis of Ni/MgO dual functional materials at room temperature for CO2 capture and methanation. *Chemical Engineering Journal* **481**, (2024).
22. Wu, X. *et al.* An investigation of the Ni/carbonate interfaces on dual function materials in integrated CO_2 capture and utilisation cycles. *Appl Catal B* **338**, (2023).
23. Huang, P. *et al.* Influence of reduction conditions on the structure-activity relationships of $NaNO_3$-promoted Ni/MgO dual function materials for integrated CO_2 capture and methanation. *Chemical Engineering Journal* **467**, (2023).
24. Porta, A. *et al.* Ru-Ba synergistic effect in dual functioning materials for cyclic CO_2 capture and methanation. *Appl Catal B* **283**, (2021).
25. Sun, S., Sun, H., Guan, S., Xu, S. & Wu, C. Integrated CO_2 capture and methanation on Ru/CeO_2-MgO combined materials: Morphology effect from CeO_2 support. *Fuel* **317**, (2022).
26. Chai, K. H., Leong, L. K., Wong, D. S. H., Tsai, D. H. & Sethupathi, S. Effect of CO_2 adsorbents on the Ni-based dual-function materials for CO_2 capturing and in situ methanation. *Journal of the Chinese Chemical Society* **67**, 998–1008 (2020).
27. Lv, Z. *et al.* Integrated CO2 capture and In-Situ methanation by efficient dual functional Li_4SiO_4@Ni/CeO_2. *Sep Purif Technol* **309**, (2023).
28. García-Bordejé, E., Belén Dongil, A., Conesa, J. M., Guerrero-Ruiz, A. & Rodríguez-Ramos, I. Dual functional materials based on Ni and different alkaline metals on alumina for the cyclic stepwise CO_2 capture and methanation. *Chemical Engineering Journal* **472**, (2023).
29. García-Bordejé, E. *et al.* Cyclic performance in CO_2 capture-methanation of bifunctional Ru with different base metals: Effect of the reactivity of COx ad-species. *Journal of CO2 Utilization* **68**, (2023).
30. Chen, L., Liu, D. & Wei, G. Performance of Na-Ru/Al_2O_3 dual function material for integrated CO_2 capture and methanation with the presence of coal ashes. *Energy Convers Manag* **299**, (2024).
31. Jeong-Potter, C. & Farrauto, R. Feasibility Study of Combining Direct Air Capture of CO_2 and Methanation at Isothermal Conditions with Dual Function Materials. *Appl Catal B* **282**, (2021).
32. Faria, A. C. *et al.* Cyclic operation of CO_2 capture and conversion into methane on Ni-hydrotalcite based dual function materials (DFMs). *Journal of CO2 Utilization* **72**, (2023).
33. Sun, H. *et al.* Understanding the interaction between active sites and sorbents during the integrated carbon capture and utilization process. *Fuel* **286**, (2021).
34. Onrubia-Calvo, J. A., Pereda-Ayo, B., González-Marcos, J. A. & González-Velasco, J. R. Lanthanum partial substitution by basic cations in $LaNiO_3$/CeO_2 precursors to raise DFM performance for integrated CO_2 capture and methanation. *Journal of CO2 Utilization* **81**, (2024).
35. Wei, L. *et al.* Nitrate-promoted gas–solid reactions of H_2 and $CaCO_3$ for mid-temperature integrated CO_2 capture and methanation. *Chemical Engineering Journal* **493**, (2024).
36. Tsiotsias, A. I. *et al.* CO_2 capture and methanation using Ru/Na_2O/Al_2O_3 dual-function materials: Effect of support synthesis method and Ru load. *J Environ Chem Eng* **12**, (2024).
37. Huang, P., Chu, J., Zhang, Z., Zhao, C. & Guo, Y. Optimizing alkali metal Salt-Induced structural assembly of Ni-MgO dual function materials for enhanced CO_2 capture and methanation performance. *Chem Eng Sci* **294**, (2024).
38. Miyazaki, S. *et al.* Continuous CO_2 Capture and Selective Hydrogenation to CO over Na-Promoted Pt Nanoparticles on Al_2O_3. *ACS Catal* **12**, 2639–2650 (2022).
39. Li, L. *et al.* Rb-Ni/Al_2O_3 as dual functional material for continuous CO_2 capture and selective hydrogenation to CO. *Chemical Engineering Journal* **477**, (2023).
40. Bobadilla, L. F., Riesco-García, J. M., Penelás-Pérez, G. & Urakawa, A. Enabling continuous capture and catalytic conversion of flue gas CO_2 to syngas in one process. *Journal of CO2 Utilization* **14**, 106–111 (2016).
41. Sun, H. *et al.* Dual functional catalytic materials of Ni over Ce-modified CaO sorbents for integrated CO_2

capture and conversion. *Appl Catal B* **244**, 63–75 (2019).

42. Shao, B. *et al.* Heterojunction-redox catalysts of $Fe_XCo_yMg_{10}CaO$ for high-temperature CO_2 capture and in situ conversion in the context of green manufacturing. *Energy Environ Sci* **14**, 2291–2301 (2021).
43. Wang, G. *et al.* Ni-CaO dual function materials prepared by different synthetic modes for integrated CO_2 capture and conversion. *Chemical Engineering Journal* **428**, (2022).
44. Ma, X. *et al.* Metal oxide-doped Ni/CaO dual-function materials for integrated CO_2 capture and conversion: Performance and mechanism. *AIChE Journal* **69**, (2023).
45. Hyakutake, T., Van Beek, W. & Urakawa, A. Unravelling the nature, evolution and spatial gradients of active species and active sites in the catalyst bed of unpromoted and K/Ba-promoted Cu/Al_2O_3 during CO_2 capture-reduction. *J Mater Chem A Mater* **4**, 6878–6885 (2016).
46. Sasayama, T. *et al.* Integrated CO_2 capture and selective conversion to syngas using transition-metal-free Na/Al_2O_3 dual-function material. *Journal of CO2 Utilization* **60**, (2022).
47. Sun, S. *et al.* Integrated CO_2 capture and utilization with CaO-alone for high purity syngas production. *Carbon Capture Science and Technology* **1**, (2021).
48. Jo, S. Bin *et al.* CO_2 green technologies in CO_2 capture and direct utilization processes: methanation, reverse water-gas shift, and dry reforming of methane. *Sustain Energy Fuels* **4**, 5543–5549 (2020).
49. Hu, Y. *et al.* MxOy (M = Mg, Zr, La, Ce) modified Ni/CaO dual functional materials for combined CO2 capture and hydrogenation. *Int J Hydrogen Energy* **48**, 24871–24883 (2023).